

DMD # 69823

Title Page

Biotransformation and Rearrangement of Laromustine

Alaa-Eldin F. Nassar, Adam V. Wisnewski, Ivan King

School of Medicine, Department of Internal Medicine, Yale University, New Haven, CT
(AFN and AVW) , Department of Chemistry, 55 N. Eagleville Rd., University of
Connecticut, Storrs, CT (AFN), Metastagen, Inc., Wilmington, DE, United States (IK).

Running Title Page

Running title: *In vitro* metabolism studies of laromustine (VNP40101M)

Corresponding Author:

Ala F. Nassar, Ph.D.
Yale University
School of Medicine
300 Cedar St/TAC s416
New Haven, CT 06510
Tel: 203-809-9608
E-mail: ala.nassar@yale.edu

Document Summary:

Number of text pages: 31
Number of tables: 4
Number of schemes: 2
Number of figures: 9
Number of references: 36
Number of words in the Abstract: 250
Number of words in the Introduction: 1517
Number of words in the Discussion: 1489

Abbreviations: Laromustine (1,2-bis(methylsulfonyl)-1-(2-chloroethyl)-2-(methylamino) carbonyl hydrazine), 90CE (1,2-bis(methylsulfonyl)-1-(2-chloroethyl) hydrazine), Lomustine or CCNU (1-(2-chloroethyl)-3-cyclohexyl-1-nitroso-urea), Carmustine or BCNU (1,3-bis(2-chloroethyl)-1-nitroso-urea), Cyclophosphamide (*N,N*-bis(2-chloroethyl)-1,3,2-oxazaphosphinan-2-amine 2-oxide), Ifosfamide (*N*,3-Bis(2-chloroethyl)-1,3,2-oxazaphosphinan-2-amide 2-oxide), AGT, O6-alkylguanine-DNA-

DMD # 69823

alkyltransferase; AML, acute myelogenous leukemia; amu, atomic mass unit; C-7, VNP40107 (a metabolite of laromustine); 90CE, a pharmacologically active degradation product of laromustine (VNP40101M) (a.k.a. VNP4090CE and, in this study, C-8); CYP, cytochrome P450; DMSO, dimethyl sulfoxide; E. coli, Escherichia coli; FDA, Food & Drug Administration; FMO, flavin-containing monooxygenase; LC-MS/MS, liquid chromatography-tandem mass spectrometry; NADPH, nicotinamide adenine dinucleotide phosphate, LC-MSⁿ; Liquid chromatography-multi-stage mass spectrometry, idiosyncratic drug reactions, IDRs; glutathione; GSH, *N*-acetylcysteine; NAC, cysteine; CYS, and hydrogen-deuterium exchange; H-D.

ABSTRACT

This review highlights the recent research into the biotransformations and rearrangement of the sulfonylhydrazine alkylating agent laromustine. Incubation of [¹⁴C]laromustine with rat, dog, monkey and human liver microsomes produced eight radioactive components (C-1 to C-8). There was little difference in the metabolite profile among the species examined, partly because nicotinamide adenine dinucleotide phosphate (NADPH) was not required for the formation of most components, but rather involved decomposition and/or hydrolysis. The exception was C-7, a hydroxylated metabolite, largely formed by CYP2B6 and CYP3A4/5. Liquid chromatography-multi-stage mass spectrometry (LC-MSⁿ) studies determined that collision-induced dissociation, and not biotransformation or enzyme catalysis, produced the unique mass spectral rearrangement. Accurate mass measurements performed with a Fourier-transform ion cyclotron resonance mass spectrometer (FTICR-MS) significantly aided determination of the elemental compositions of the fragments, and in the case of laromustine, revealed the possibility of rearrangement. Further, collision-induced dissociation produced the loss of nitrogen (N₂), methylsulfonyl and methyl isocyanate moieties. The rearrangement, metabolite/decomposition products and conjugation reactions were analyzed utilizing hydrogen-deuterium exchange (H-D), exact mass, ¹³C-labeled laromustine, nuclear magnetic resonance spectroscopy (NMR) and LC-MSⁿ experiments to assist with the assignments of these fragments and possible mechanistic rearrangement. Such techniques produced valuable insights into these

DMD # 69823

functions: (1) P450 is involved in C-7 formation but plays little or no role in the conversion of [¹⁴C]laromustine to C-1 through C-6 and C-8; (2) the relative abundance of individual degradation/metabolite products was not species dependent; and (3) laromustine produces several reactive intermediates that may produce the toxicities seen in the clinical trials.

Introduction

Alkylating agents are capable of introducing an alkyl group into nucleophilic sites on DNA or RNA through covalent bonds (Alkylating Agents, 2014). There are several groups of alkylating agents such as nitrogen mustards (e.g., mechlorethamine, cyclophosphamide, ifosfamide, chlorambucil, bendamustine, and melphalan); ethylenimines (e.g., thio-tepa); nitrosoureas (e.g., carmustine, lomustine, streptozocin); triazines (e.g., dacarbazine, temozolomide); methylhydrazines (e.g., procarbazine); and alkyl sulfonates (e.g., busulfan). Originally, alkylating agents were best known for their use as mustard gas and related chemical weapons in World War I, due to their toxicity. These agents are thought to react with the N7 position of guanine or any nitrogen base in each of the double strands of DNA, resulting in damage to the DNA (Alkylating Agents, 2014). They are harmful to normal cells, especially cells that divide frequently, such as those in the gastrointestinal tract, bone marrow, testicles and ovaries, which can cause loss of fertility. As early as the 1940's, it was discovered that they could be used as part of chemotherapy in different types of cancers (Scott 1970, Wiedemann et.al., 1996, Goodman et al., 1946). One early example is busulfan, a cancer drug in use since 1959; in 1999 it was approved by the US Food and Drug Administration (FDA) for treatment of chronic myeloid leukemia (CML). Busulfan was the main chemotherapeutic for treatment of chronic myeloid leukemia (CML) until it was displaced by imatinib, but it is still in use because of its low cost. Alkylating agents are commonly used to treat many different cancers, including leukemia, lymphoma, Hodgkin's disease, multiple myeloma, and sarcoma, as well as cancers of the lung,

DMD # 69823

breast, and ovary. The risk with these drugs is that, at higher doses, they can cause long-term damage to the bone marrow.

One key to successful drug design and development lies in finding the right combination of diverse properties such as activity, toxicity, exposure, etc. Continued development of any drug candidate hinges on the research team being able to determine, and then optimize, these exposure-activity-toxicity relationships. Therefore, the goal of drug metabolism research is to optimize plasma half-life, drug/metabolic clearance, metabolic stability, and the ratio of metabolic to renal clearance. Concurrently, the researcher must be aware of the need to minimize or eliminate issues such as gut/hepatic-first-pass metabolism, inhibition/induction of drug metabolizing enzymes by metabolites, biologically active metabolites, metabolism by polymorphically expressed drug metabolizing enzymes, and formation of reactive metabolites. A successful outcome is a safer drug that undergoes predictable metabolic inactivation or even undergoes no metabolism. Approaches available to the drug design team, as they seek to meet the above goals, include active metabolites, prodrugs, hard and soft drugs; these will be discussed below, with some examples from recent case studies.

The prodrug approach is commonly used in drug design. Prodrugs undergo an enzymatic and/or chemical transformation *in vivo* to release the active drug. They help researchers to improve the physicochemical, biopharmaceutical or pharmacokinetic properties of pharmacologically potent drugs. About 10% of drugs approved worldwide can be classified as prodrugs (Rautio et al., 2008). Prodrugs were discovered when it was demonstrated that the antibacterial agent protosil was active *in vivo* only when it

DMD # 69823

was metabolized to the actual drug sulfanilamide. Prodrugs most commonly use either oxidative or reductive activation; for example, protosil is activated by reduction of its azo linkage to the amine sulfa drug. Another example of a prodrug is the antipyretic agent phenacetin, which becomes active upon conversion to acetaminophen. Carbamazepine is an anticonvulsant drug that is the metabolic precursor of the active agent carbamazepine 10,11-oxide. Minoxidil, originally developed as a potent vasodilator, also induces hypertrichosis of facial and body hair (Buhl et al., 1990). Research data shows that sulfation is a critical step for the hair-growth effects of minoxidil and that it is the sulfated metabolite that directly stimulates hair follicles.

The various structural modifications of ampicillin demonstrate how the prodrug strategy can improve pharmacokinetics (PK) properties. Pivampicillin, talampicillin, and bacampicillin are prodrugs of ampicillin, each of which is produced from the esterification of the polar carboxylate group to form lipophilic, enzymatically labile esters (Sjövall et al., 1978, Ensink et al., 1996, Ehrnebo et al., 1979). These prodrugs result in nearly total absorption, whereas that of ampicillin is <50%. A randomized cross-over study on 11 healthy volunteers to determine the pharmacokinetics of bacampicillin, ampicillin and pivampicillin showed that the relative bioavailability of bacampicillin (%F = 87-95) and pivampicillin (%F = 82-89) was comparable, whereas ampicillin was less than 2/3 that of the others (%F = 47-49). Additionally, the mean of the individual peak concentrations in serum was 8.3 µg/ml for bacampicillin, 7.1 µg/ml for pivampicillin and 3.7 µg/ml for ampicillin.

DMD # 69823

The prodrug strategy has played an important role in developing alkylating antineoplastic agents as anti-cancer drugs over the past few decades. An ideal cancer chemotherapeutic prodrug is inactive until metabolized by a tumor-specific enzyme. Cyclophosphamide and ifosfamide, which are nitrogen mustards, are examples of anticancer prodrugs metabolized by cytochrome P450 pathways (Ortiz de Montellano 2013) and their active metabolites which are subsequently formed once they have entered the cells. Scheme 1 shows the activation pathway of cyclophosphamide and ifosfamide. Carmustine and lomustine are spontaneously decomposed (non-enzymatic) to the active compound (Colvid et al., 1974 and Brundrett et al., 1976). Scheme 2 shows the degradation products of two nitrosoureas: carmustine and lomustine.

Laromustine [VNP40101M, 1,2-bis(methylsulfonyl)-1-(2-chloroethyl)-2-(methylamino)carbonylhydrazine] is an active member of a relatively new class of sulfonylhydrazine prodrugs under development as antineoplastic alkylating agents (Penketh et al., 2004; Baumann et al., 2005). Figure 1a shows the chemical structure of laromustine and its active degradation product VNP4090CE (90CE). Two distinct types of reactive intermediates, 90CE and methylisocyanate, are generated as shown in Fig. 1b. Hard chloroethylating (DNA-reactive) species such as 90CE alkylate DNA at the O^6 -position of guanine residues that progress to G-C interstrand cross-links as shown in Fig. 1b (Penketh et al., 2000, 2004). Methylisocyanate, a soft electrophilic carbamoylating agent, binds preferentially and stoichiometrically to sulfhydryl groups and inhibits a number of enzymes, including O^6 -alkylguanine-DNA-alkyltransferase

DMD # 69823

(AGT), a DNA repair enzyme. Laromustine surpasses other similar agents in that it generates both 90CE and methylisocyanate (Baumann et al., 2005). It is thought that the antineoplastic effect of 90CE and related chloroethylating species augments the release of methylisocyanate and its inhibition of DNA repair by AGT, likely producing the significant improvement of antineoplastic activity of laromustine relative to that of other sulfonylhydrazine alkylating agents. It showed anticancer activity against a broad spectrum of transplanted tumors (Finch et al., 2001) and exhibited antileukemic activity in initial clinical trials (Giles et al., 2004). The average human plasma C_{max} for laromustine is approximately 25 μ M (Nassar et al., 2009).

Elderly patients with de novo poor-risk acute myelogenous leukemia (AML) achieved durable complete remissions with Laromustine injection; thus it offers an important therapeutic option for such patients. As an example, eighty-five patients age 60 years or older (median age, 72 years; range, 60 to 87 years) with previously untreated poor-risk AML were treated with laromustine. Nearly all (96%) had at least two risk factors, with 39% having four or more risk factors. Median overall survival was 3.2 months, with a 1-year survival of 21%. Among those who achieved complete response (CR)/CR with incomplete platelet recovery the median duration of survival for (CRp) was 12.4 months, and 1-year survival 52% (Schiller et al., 2010).

The use of mass spectrometry has become vital to assessment of structure information in complex biological matrices (Baillie 1992; Watt et al., 2003; Mutlib et al., 1995; Pochapsky and Pochapsky 2001; Nassar et al., 2003a and 2003b). Time-of-flight MS, FTICR-MS, and Orbitrap mass spectrometers are among the most effective for this

DMD # 69823

work. With recent advances in FTICR-MS, it has become routine to generate mass spectra with ppm mass accuracy and exceptional resolving power, two metrics which are critical to determining fragmentation ions for metabolite identification for drug metabolism studies. The online H-D method was developed for use with small molecules where online exchange on column without any further sample preparation is employed for metabolite identification and characterization. H-D has become common practice for online analysis of metabolite identification of complex matrices; when combined with modern mass spectrometry, it has proven ideal for the task of structure confirmation (Nassar et al., 2003a, 2003b and 2004).

Herein we summarize and review several *in vitro* studies that were designed to examine the biotransformation and rearrangement of laromustine. High mass accuracy and ultrahigh resolution measurements (Nassar et al., 2010a and 2010b), H-D, stable-isotope labeled analogue (^{13}C -labeled laromustine), NMR, and detailed analyses of the LC-MSⁿ experiments were used to assist with the assignments of these fragments and possible mechanistic rearrangement. This work was valuable in this research because it provided significantly enhanced guidance into the mechanistic rearrangement of laromustine. These studies revealed that laromustine undergoes rearrangement, dehalogenation, and hydrolysis at physiological pH to form active moieties. Laromustine (VNP40101M) produces several reactive metabolites which were trapped by glutathione (GSH), *N*-acetylcysteine (NAC), and cysteine (CYS) in the *in vitro* systems (Nassar et al., 2011).

1. *In vitro* studies

1.1 *In vitro* metabolism of [¹⁴C]laromustine. The *in vitro* profile of [¹⁴C]laromustine metabolites/degradation products formed by liver microsomes from rats, dogs, monkeys and humans is shown in Fig. 2. When [¹⁴C]laromustine (100 μM) was incubated with these four liver microsomes in the presence of NADPH, eight radioactive components (C-1 through C-8) were detected after 60 minutes of incubation (Fig. 2). The metabolite profile was similar for all species with two notable exceptions: First, rat liver microsomes formed C-3 at low levels or not at all, and second, dog and monkey liver microsomes produced considerably higher levels of C-7 compared with rat and human liver microsomes. Component C-8 cochromatographed (RT ~ 39 min) with an authentic standard of 90CE; it was a major component at early time points and at low substrate concentrations regardless of the source of liver microsomes. Formation of 90CE (C-8) is associated with formation of methylisocyanate, but formation of methylisocyanate from [¹⁴C]laromustine was not detected by radiometric HPLC because it lacked the ¹⁴C-label, which is part of the chloroethyl moiety, as shown in Fig. 1a.

The differences between the presence and absence of NADPH are summarized in Supplemental Tables 1 through 3. In the presence of NADPH, after 60 min of incubation, the loss of substrate for rat, dog, monkey and human liver microsomes was 63, 82, 76 and 64% respectively, and mass balance ranged from 91.0 – 99.3%. In the absence of NADPH, after 60 min of incubation with [¹⁴C]laromustine (100 μM), the loss of substrate for rat, dog, monkey and human liver microsomes was 59, 53, 61 and 59% respectively, and mass balance ranged from 100.6 – 116.4%. For rat, dog, monkey and

DMD # 69823

human liver microsomes, the total formation (sum of C-1, C-2, C-3, C-4 and C-7) was 54, 81, 70 and 55% respectively in the presence of NADPH and 59, 69, 66 and 64%, respectively, in the absence of NADPH.

Of the radioactive components detected, only the formation of C-7 was dependent on NADPH. Formation of C-7 involved methyl-hydroxylation of laromustine (+16 amu) on the methylisocyanate moiety. The time course of C-7 formation by liver microsomes from each species indicates that once formed, C-7 is further metabolized or degraded. The rate of formation of C-7 followed the rank order (from fastest to slowest): Dog \approx monkey $>$ rat \approx human, which corresponds to the same rank order for the overall rate of laromustine consumption. Formation of C-7 did not account for the loss of parent compound. The loss of substrate was largely caused by non-enzymatic chemical degradation. In contrast, formation of C-7 was not observed in zero-cofactor (no NADPH) and zero-protein samples, suggesting its formation was enzymatic.

In vitro studies were designed to determine the role of P450 and other HLM enzymes on laromustine metabolism. Incubations of [^{14}C] laromustine were performed with and without human liver microsomes and with boiled (denatured) microsomes, with and without NADPH. The data suggested that [^{14}C] laromustine undergoes extensive chemical degradation rather than metabolism by cytochrome P450s. It was also determined that reactions stopped with methanol, acetonitrile and perchloric acid generated similar degradation profiles. This suggests that the sample preparation methods did not contribute to the degradation products.

1.2 Identification of human CYP enzymes involved in the metabolism of [¹⁴C]laromustine. To identify the human CYP enzyme or enzymes responsible for C-7 formation, laromustine (25 and 100 μM) was incubated with a bank (n = 10) of individual samples of human liver microsomes (correlation analysis) and a panel of recombinant human enzymes. Of the recombinant human enzymes evaluated, only CYP2B6 and CYP3A4/5 converted laromustine to C-7, and did so at comparable rates. With the recombinant CYP enzymes, C-7 formation was evaluated at a single time point (10 min) based on time-course experiments with human liver microsomes. We cannot exclude the possibility that one or more recombinant CYP enzymes formed C-7 at a later or earlier time point. As shown in Fig. 3, the sample-to-sample variation in the conversion of [¹⁴C]laromustine (25 μM) to C-7 correlated strongly (r = 0.923) with CYP2B6 (bupropion hydroxylase) activity. It also correlated weakly with CYP3A4/5 activity based on testosterone 6β-hydroxylation (r = 0.572) and midazolam 1'-hydroxylation (r = 0.461). The linear regression lines for CYP2B6 and CYP3A4/5 did not pass through or near the origin, suggesting that both enzymes are involved in the formation of C-7. The correlation between C-7 formation and CYP2B6 activity (r = 0.923) improved when the variation in CYP3A4/5 activity was also taken into consideration (r = 0.945).

[¹⁴C]laromustine (25 and 100 μM) was incubated with a panel of recombinant human CYP enzymes (rCYP1A2, 2A6, 2B6, 2C8, 2C9, 2C19, 2D6 and 3A4) and recombinant human FMO3 for zero and 10 min, as summarized in Table 1, and Supplemental Tables 4 and 5. Among the panel of recombinant human CYP and FMO enzymes evaluated, formation of C-7 was only observed in incubations with

DMD # 69823

recombinant CYP2B6 and CYP3A4. Loss of parent compound was observed in all incubations including the control samples (*i.e.*, samples containing membranes with no human CYP enzyme). Formation of C-7 was observed in incubations containing recombinant human CYP2B6 and CYP3A4 at both substrate concentrations. After 10-min incubations of [¹⁴C]laromustine at concentrations of 25 and 100 μM with recombinant human CYP2B6, the [¹⁴C] quantities of C-7 were 376 and 513 pmol, respectively. After 10-min incubations of [¹⁴C]laromustine at concentrations of 25 and 100 μM with recombinant human CYP3A4, the [¹⁴C] levels of C-7 were 362 and 549 pmol, respectively. The formation of the radioactive components increased with respect to incubation time with the exception of C-7. The formation of C-7 tended to increase with increasing incubation time and protein concentration; however, formation of C-7 was not linear with respect to either of these parameters. In addition, the formation of C-7 was not proportional to substrate concentration. The non-linearity of C-7 formation suggests that, once formed, this component was further metabolized or degraded.

2. Novel Rearrangement

2.1 Unanticipated loss of N₂ from laromustine by collision-induced dissociation. During metabolism studies of laromustine utilizing liquid chromatography-mass spectrometry, a novel mass spectral rearrangement by collision-induced dissociation in the positive ion mode was observed. Accurate mass measurements were performed with a Fourier transform ion cyclotron resonance-mass spectrometer (FTICR-

DMD # 69823

MS) to determine the elemental compositions of the fragments. During the fragmentation of m/z 171 to m/z 143 direct cleavage fragment ions were not observed, leading to the speculation that laromustine undergoes rearrangement. This suggested the loss of nitrogen (N_2), methylsulfonyl and methyl isocyanate moieties from laromustine by collision-induced dissociation. Additionally, the rearrangement was analyzed utilizing hydrogen-deuterium exchange (H-D), a stable-isotope labeled analogue (^{13}C -labeled laromustine), and LC-MSⁿ experiments to assist with the assignments of these fragments and possible mechanistic rearrangements. A mechanism for this rearrangement was proposed on the basis of fragmentation ions. H-D exchange methods are useful for determination of the presence, number, and position of H-D exchangeable functional groups on metabolite structures and thus serve as an aid for structural elucidation of metabolites, as well as aiding in differentiation of compounds (Nassar 2003a). It has been reported that H-D exchange can be used to discriminate between N- or S-oxide formation and monohydroxylation; also, conjugation such as glucuronide can be easily identified with this technique. However, in this study the samples were dried under a nitrogen stream and then reconstituted in D₂O mobile phase for the H-D exchange. Stable isotopes have the same number of protons as common elements, and consequently share the same physicochemical properties, but they differ in mass due to a difference in the number of neutrons. Stable isotope labeling involves the use of non-radioactive isotopes that can be used to confirm metabolites. Stable isotope labeling provides great improvements and enhanced confidence in metabolite identification and characterization (Kassahun et al., 2001). The combination

of these two approaches (H-D and stable isotopes) provides a comprehensive understanding of structure elucidation.

2.2 Analysis with Fourier transform ion cyclotron resonance-mass spectrometry (FTICR-MS). Each sample was analyzed in triplicate. Exact mass measurement of the peak of interest (observed at m/z 325) was initially collected. Subsequently, the peak of interest was selected and fragmented by collision induced dissociation (CID) to produce product ions. Bruker Daltonics DataAnalysis software (v. 3.4) was used to analyze the data and assignments were made based on exact mass measurements and fit of isotopic peaks to that of theoretical isotopic patterns. After generation of the m/z mass spectrum for this peak, data was deconvoluted to determine monoisotopic masses. The data are shown in Table 2 and Fig. 4. The mass errors were between -1.64 to 2.12 ppm as shown in Table 2. These data allowed us to determine the elemental compositions of the fragmentation ions of laromustine and provided unambiguous fragmentation ion pathways.

2.3 Confirmation of the fragmentation ions of laromustine. Sequential LC-MSⁿ experiments were carried out on a LTQ ion trap mass spectrometer to gain extensive structural information for laromustine in full scan MS mode. The fragmentation ions from the initial MSⁿ experiments on laromustine using LTQ suggested that rearrangement of laromustine took place. Supplemental Figure 1 shows the sequential MSⁿ experiments up to MS⁵. Under the experimental conditions presented (Nassar et

DMD # 69823

al., 2010b), and on the basis of the MS⁵ results, direct cleavage fragment ions were not observed; then it was speculated that laromustine undergoes rearrangement during the fragmentation of ion m/z 171 to m/z 143. The MS signature of chlorine isotope (³⁵Cl and ³⁷Cl) in laromustine was observed and verified in the fragmentation ions; this unique signature confirmed the formation of m/z 143. Also the fragmentation ions were further confirmed using H-D exchange and stable-isotope experiments.

The proposed mechanism of formation for the fragmentation ions m/z 251, m/z 171, m/z 143, m/z 107, m/z 81, and m/z 63 is shown in Fig. 5. The product-ion spectra of m/z 325 showed the fragment ions of m/z 308, 273, 251, 143, 107, 93, 81, and 63. The fragment ion at m/z 308 resulted from the loss of ammonia from m/z 325. The fragment ion at m/z 273 resulted from the losses of HCl from m/z 308. The fragment ion at m/z 251 resulted from cleavage of the C-N bond. The fragment ion at m/z 143 resulted from the loss of CH₃SO₂H and N₂ from m/z 251. The fragment ion at m/z 107 was due to losses of HCl from m/z 143. The fragment ion at m/z 81 was due to losses of C₂H₃Cl from m/z 143. The product-ion spectra of m/z 327 (laromustine, ¹³C₂) showed the fragment ions of m/z 310, 253, 145, 109, 95 and 65. The product-ion spectra of m/z 330 using H-D exchange experiments showed the fragment ions of m/z 310, 253, 144, and 95. Detailed analyses of the LC-MSⁿ mass spectra suggest that the fragmentation process involves a rearrangement. This rearrangement fragment provided important clues about the location and identity of functional groups of laromustine. This was very useful for elucidating ionic structures of laromustine. Proposed fragmentation

DMD # 69823

mechanisms for m/z 325 (laromustine), m/z 327 (laromustine, $^{13}\text{C}_2$), and m/z 330 (laromustine, H-D) are shown in Fig. 6.

3. Identification and characterization of *in vitro* metabolite/decomposition products of laromustine in HLM. Eight metabolite/decomposition products along with the parent drug were detected following incubation of laromustine with human liver microsomes for 60 min in the presence of NADPH. The major decomposition products were designated C-1 and C-4. Table 3 shows the molecular formula, molecular weights, retention times, results from H-D exchange experiments, *N*-rule data and RDBE data of the metabolite/decomposition products of laromustine formed in HLM incubations. Peak C-2 was not identified because the MS spectrum of C-2 was not well ionized under the conditions utilized in this study. C-6 product was not reported because it is one of the potential impurities in laromustine (Nassar et al., 2010a). The total conversion (sum of C-1, C-2, C-3, C-4 and C-7) of laromustine in HLM was 55%, in the presence of NADPH after 60 min; data are shown graphically in Fig. 2. *In vitro* studies using HLM have shown that C-7 formation is mediated primarily by CYP3A4/5 and CYP2B6 (Nassar et al., 2009).

3.1. Identification and characterization of C-1: The MS spectrum of C-1 was acquired, which revealed an ammonium adducted, protonated molecular ion $[\text{M}+\text{NH}_4]^+$ at m/z 142. Comparison of the full-scan mass spectrum of undeuterated/deuterated C-1 enabled the determination of the number of labile protons. The full-scan mass spectrum

DMD # 69823

of undeuterated/deuterated C-1 gave ions at m/z 142/147 respectively, which suggested C-1 has only one labile proton. The stable-isotopic experiments gave a full-scan ion at m/z 144, which suggested that the structure of C-1 contains $^{13}\text{C}_2$. The product-ion spectra of m/z 142 from sequential MS^n experiments showed the fragment ions of m/z 125, 107, 81, and 79. The fragment ion at m/z 125 resulted from the loss of ammonia from m/z 142. The fragment ion at m/z 107 was due to the loss of water from m/z 125. The fragment ion at m/z 79 resulted from cleavage of the C-S bond. The data in Table 3 show that C-1 contains no nitrogen (N) atoms, has only one labile proton and RDBE is equal to 0 which agrees with the proposed structure (2-(methylsulfonyl)ethanol).

3.2 Identification and characterization of C-3 and C-4: The MS spectra of C-3 and C-4 were acquired, which revealed an ammonium adducted, protonated molecular ion $[\text{M}+\text{NH}_4]^+$ at m/z 232 (Supplemental Figures 2 and 3 for components C-3 and C-4 respectively). The data in Table 3 show that C-3 and C-4 contain an even number of nitrogen (N) atoms and RDBE is equal to 1. Comparison of the full-scan mass spectrum of undeuterated/deuterated C-3 and C-4 enabled the determination of the number of labile protons. The full-scan mass spectrum of undeuterated/deuterated C-3 and C-4 gave ions at m/z 232/237 respectively, which suggested C-3 and C-4 have one labile proton. The stable-isotopic experiments gave a full-scan ion at m/z 234 for C-3 and C-4, which suggested that the structure of C-3 and C-4 contains $^{13}\text{C}_2$. Stable-isotopic experiments, in addition to supporting data including N -rule, RDBE, and MS^n , provided evidence to support the structural characterization of C-3 and C-4. The product-ion

DMD # 69823

spectra of C-3 (Supplemental Figure 2B and C) and C-4 (Supplemental Figure 3B and C), from sequential MSⁿ experiments, showed the fragment ions of *m/z* 232 to be *m/z* 215, 135, and 81. The fragment ion at *m/z* 215 resulted from the loss of ammonia from *m/z* 232. The fragment ion at *m/z* 135 was due to losses of CH₃SO₂H moiety from *m/z* 215. The fragment ion at *m/z* 81 resulted from cleavage of the N-S bond (Supplemental Figure 4). The proposed structure for C-3 and C-4 is (E)-N'-(2-(methylsulfonyl)ethylidene) methanesulfonohydrazide (isomer) (Supplemental Figure 4).

3.3 Identification and characterization of C-5: The MS spectrum of C-5 was acquired, which revealed an ammonium adducted, protonated molecular ion [M+NH₄]⁺ at *m/z* 232. Comparison of the full-scan mass spectrum of undeuterated/deuterated C-5 enabled the determination of the number of labile protons. The full-scan mass spectrum of undeuterated/deuterated C-5 gave ions at *m/z* 232/236 respectively, which suggested C-5 has no labile proton. The stable-isotopic experiments gave a full-scan ion at *m/z* 234, which suggested that the structure of C-5 contains ¹³C₂. The product-ion spectra of *m/z* 232 from sequential MSⁿ experiments showed fragment ions of *m/z* 215, 135, 81 and 57. The fragment ion at *m/z* 215 resulted from the loss of ammonia from *m/z* 232. The fragment ion at *m/z* 135 was due to loss of the CH₃SO₂H moiety from *m/z* 215. The fragment ion at *m/z* 81 resulted from cleavage of the N-S bond (Supplemental Figure 5). The data in Table 1 show that C-5 contains an even number of nitrogen (N) atoms, no labile proton, and RDBE is equal to 1, which agrees with the proposed structure (1-(methylsulfonyl)-2-(2-(methylsulfonyl)ethyl)diazene).

3.4 Identification and characterization of C-7: This component was detected when larmustine was incubated with HLM in the presence of NADPH, suggesting that this is a metabolite rather than a decomposition product (Fig. 2). The fact that C-7 decreased over the incubation time suggests that C-7 continued to metabolize or decompose. The MS spectrum of C-7 was acquired, which revealed an ammonium adducted, protonated molecular ion $[M+NH_4]^+$ at m/z 341, 16 Da (dalton) more than the parent drug, suggesting the addition of oxygen on larmustine. The presence of pseudomolecular ions $[M+NH_4]^+$ at m/z 341/343 in a ratio of 3:1 suggested the presence of chlorine on the molecule. The MS signature of chlorine in C-7 was verified by multi-stage MS. The product-ion spectra of m/z 341 from sequential MS^n experiments showed the fragment ions of m/z 306, 294, 251, 227, 148, 143, and 93. The fragment ion at m/z 306 resulted from the loss of ammonia and water from m/z 341. The fragment ion at m/z 227 was due to the loss of CH_3SO_2 moiety from m/z 306. The fragment ion at m/z 148 was due to the loss of CH_3SO_2 moiety from m/z 227. The fragment ion at m/z 251 resulted from cleavage of the C-N bond. The fragment ion at m/z 143 resulted from the loss of CH_3SO_2H and N_2 moieties from m/z 251. The stable-isotopic experiments gave a full-scan ion at m/z 343. These observations support the proposed structure of C-7. The unique MS signature of chlorine isotope ratios that differs in mass by 2 Da greatly facilitated the structure characterization. The proposed structure and fragmentation is shown in Fig. 7.

DMD # 69823

3.5 Buffer incubations. Following incubation of laromustine with phosphate buffer (50 mM) at pH 7.4 for 60 min, decomposition products along with the parent drug were detected, and were similar to those detected in HLM in the absence of NADPH.

4. Identification and characterization of *in vitro* conjugation reactions of laromustine. The retention times of conjugation reactions were between 16 and 48 min with adequate separation efficiency. Each structure was assigned a numerical notation (M-1, M-2, etc.) based on the order of HPLC elution. MSⁿ data were acquired for each structure. Following incubation of laromustine with human liver microsomes for 60 min in the presence of NADPH, GSH, CYS, and NAC, eight conjugation reactions were detected (M-1 to M-8). Following incubation of VNP4090CE with human liver microsomes for 60 min in the presence of NADPH, GSH, CYS, and NAC, five distinct conjugation reactions were detected (M-1, M-3, M-5, M-7 and M-8). M-2, M-4 and M-6 were not detected because VNP4090CE does not contain a methylformamide group (Fig. 1a). Reactive moieties (groups) formed from laromustine and VNP4090CE in HLM or buffer incubations are shown in Supplemental Table 7. The CH₃SO₂CH₂CH₂- and CH₃NHCO- groups formed conjugates with GSH, CYS, and NAC. The CH₃SO₂NHN=CHCH₂- group formed conjugates with GSH and NAC but it did not form a conjugate with CYS under the experimental conditions evaluated, suggesting that CYS has low trapping efficiency with the CH₃SO₂NHN=CHCH₂- group and/or this conjugate did not ionize well under the MS conditions. Table 4 shows the chemical structure, molecular weight, retention time, and results from H-D experiments on the conjugation

DMD # 69823

reactions. These conjugates were formed in buffer solution with or without HLM, indicating that the formation of active moieties from larmustine and VNP4090CE was enzyme independent. The MS data from buffer incubations gave a stronger MS^n signal because the buffer has less isobaric interferences than HLM.

4.1. Identification and characterization of M-3 as an example of how we identified M1-M8. The LC-MS retention time of M-3 was approximately 27.6 min, and the mass spectrum revealed a protonated molecular ion $[M+H]^+$ at m/z 414, suggesting that the $CH_3SO_2CH_2CH_2-$ group was covalently linked to the sulfur atom of the GSH moiety (Supplemental Figure 6). The absence of pseudomolecular ions $[M+H]^+$ at m/z 414/416 in a ratio of 3:1 suggested that M-3 does not contain chlorine. The stable-isotopic experiments (^{13}C -labeled) gave a full-scan ion at m/z 416, suggesting that M-3 contains $[^{13}C]$. The H-D experiments gave a full-scan ion at m/z 421, suggesting there are 6 labile protons on M-3. The product-ion spectra of m/z 414 showed the fragment ions of m/z 339, 285, 268, 250, 240, 193, 113, and 107 (Supplemental Figure 6). The fragment ion at m/z 339 resulted from the loss of $C_2H_5NO_2$ from m/z 414. The fragment ion at m/z 285 was due to the loss of the glutamate moiety from m/z 414. The fragment ion at m/z 268 resulted from the loss of NH_3 from m/z 285. The fragment ion at m/z 250 resulted from the loss of H_2O from m/z 268. The fragment ion at m/z 240 resulted from the loss of CO from m/z 268. The fragment ion at m/z 193 resulted from the loss of $C_2H_5NO_2$ from m/z 268. The fragment ion at m/z 113 resulted from the loss of CH_3SO_2H from m/z 193. The fragment ion at m/z 107 resulted from cleavage of the C-S bond.

DMD # 69823

These observations support the proposed structure of M-3 and suggest that an unusual rearrangement may occur after dehalogenation of VNP4090CE, resulting in the formation of a novel reactive intermediate. The $\text{CH}_3\text{SO}_2\text{CH}_2\text{CH}_2-$ group was trapped by GSH to form M-3. The proposed structure and fragmentation ions of M-3 based on supported data from LC-MSⁿ, *N*-rule, RDBE, stable isotope experiments, and H-D experiments are shown in Supplemental Figure 7.

5. Discussion

These studies indicate that laromustine readily undergoes base-catalyzed (non-enzymatic) conversion to methylisocyanate and 90CE, which further degrade to additional chloroethylating derivatives. Fig. 1b shows the proposed formation of decomposition/metabolite product pathways of laromustine formed in *in vitro* systems. The rate at which [¹⁴C]laromustine (100 μM) produces its metabolites/degradation products in the presence of NADPH-fortified human liver microsomes was essentially the same as that in the absence of NADPH or the presence of boiled (heat-denatured) microsomes. Additionally, it remained consistent with the non-enzymatic rate of laromustine degradation in potassium phosphate buffer (Nassar et al., 2009). This suggests that laromustine metabolism/degradation is not significantly affected by human liver microsomal CYP enzymes and carboxylesterases.

Only the formation of C-7 required the presence of NADPH. C-7 appears to be decomposed or metabolized further, which suggests that cytochrome P450 is a factor in C-7 formation but plays little or no role in the conversion of [¹⁴C]laromustine to other

DMD # 69823

radioactive products. The combination of the correlation analysis and recombinant human CYP enzyme experiments points to a role for both CYP2B6 and CYP3A4 in the formation of metabolite C-7. The formation of C-7 correlated most strongly with CYP2B6 activity, with moderate correlation to CYP2A6, CYP2D6 and CYP3A4 activity in 10 individual samples of NADPH-fortified human liver microsomes. As shown by the recombinant human CYP data, rCYP3A4 and rCYP2B6 were capable of forming C-7, whereas formation of C-7 was not observed with rCYP2A6 and rCYP2D6. Laromustine was shown to be a competitive inhibitor for both CYP2B6 and CYP3A4, which indicates that it is a substrate for these enzymes (Nassar et. al, 2009).

It was undertaken to determine whether one or more CYP enzymes in human liver microsomes can potentially contribute 25% or more to the clearance of laromustine. We examined the role of CYP2B6 and CYP3A4/5 in the hydroxylation of laromustine to C-7, which is one of eight radioactive components detected when [¹⁴C]laromustine is incubated with human liver microsomes. Studies with a panel of recombinant human CYP enzymes and correlation analysis with a bank of human liver microsomes implicated CYP2B6, and showed that C-7 is the only component whose formation is dependent on NADPH. However, inhibition of CYP2B6 and CYP3A4/5 will not impact the pharmacokinetics of laromustine. This is because the rate of loss of [¹⁴C]laromustine (100 μM) in the presence of NADPH-fortified human liver microsomes was essentially the same as that in the absence of NADPH or the presence of boiled (heat-denatured) microsomes. This rate was also consistent with the non-enzymatic rate of laromustine degradation in potassium phosphate buffer. Therefore, although

DMD # 69823

CYP2B6 and CYP3A4/5 convert laromustine to C-7, metabolism by CYP (or any other microsomal enzyme) does not contribute substantially to the overall rate of *in vitro* clearance, which is largely determined by non-enzymatic degradation (Nassar et al., 2009 and 2010c).

Laromustine undergoes a rearrangement which was determined by a combination of different methods such as exact mass measurements, stable isotope, H-D exchange and MSⁿ experiments. H-D exchange experiments were useful to determine the number of exchangeable protons in the fragmentation ions. The data from FTICR-MS facilitated the determination of the elemental compositions of the fragmentation ions of laromustine and provided unambiguous fragmentation ion pathways. The fragmentation processes are typically categorized as direct cleavage or rearrangement. Cleavage reactions are simply the breaking of a bond to produce two fragments. These reactions usually produce an even electron ion. Rearrangements are more complex reactions that involve both making and breaking bonds. These reactions are thermodynamically favorable because they require less energy. However they also require a mechanism that is not as kinetically favorable when compared to a simple cleavage reaction (McLafferty and Turecek, 1993). The distinct rearrangement fragment of laromustine was observed and provided important clues about the location and identity of its functional groups. This was very useful for elucidating the unique structures of laromustine reactions.

Laromustine undergoes extensive decomposition/metabolism in *in vitro* systems. Following incubation of [¹⁴C]laromustine with HLM in the presence of NADPH, eight

DMD # 69823

metabolite/decomposition products along with the parent drug were detected. Most of the identified structures resulted from the chemical decomposition of laromustine and were not P450-mediated. The major decomposition products (C-3, C-4 and C-5) from the incubation of laromustine in HLM were found to be the products of dehalogenation, rearrangement, and hydrolysis. Their formations do not require the involvement of any enzymes. H-D exchange, ^{13}C -labeled laromustine, NMR, and MS^n techniques were applied to identify and characterize the metabolite/decomposition components of laromustine. H-D exchange combined with MS is an efficient tool for studying metabolite identification. A combination of these techniques appears promising for maximizing structural information for laromustine.

The mechanisms of formation for the decomposition components were proposed. The major decomposition components were not P450-mediated. C-7 was only detected when laromustine was incubated with HLM in the presence of an NADPH-generating system, suggesting that this is a metabolite rather than a decomposition product. Dechlorination and hydrolysis of the methyl isocyanite moiety from laromustine does not require P450 enzymes and occurs at biological pH. A mechanism for the formation of these metabolite/decomposition products from laromustine was proposed. The structural characterizations of the MW 214 components (C-3 and C-4) were verified using NMR. NMR data suggested that peak (C-3) is composed of the free base form with a carbon-nitrogen double bond. The free base (C-3) was found to exist as a mixture of *cis* and *trans* isomers with the *trans* isomer typically more abundant. The unusual observation that the methylene protons adjacent to the double bond are exchangeable

DMD # 69823

in CD₃OD suggests that the double bond can shift in the free base to give a carbon-carbon double bond. In the presence of even weak acids, the free base form is converted to the salt which is present almost entirely in the *trans* form and does not have exchangeable methylene protons, indicating that the double bond does not shift between the carbons in the salt. The salt (C-4) elutes slightly later than the free base as shown in Fig. 2. The third MW 214 peak (C-5) could not be isolated (for NMR analysis) due to its apparent instability. This component has no exchangeable protons, suggesting that the double bond may shift to reside between the nitrogen atoms. Based on the NMR data, C-3 was determined to be the free base and C-4 was determined to be the salt form of *m/z* 232. The proposed structures and fragmentations ions for C-4 and C-5 are shown in Supplemental Figures 4 and 5. A proposed mechanism of formation of C-4 and C-5 is shown in Figure 8. It has been proposed that laromustine undergoes hydrolysis to form C-8 which then produces C-5 after dehalogenation and rearrangement. C-5 undergoes further rearrangement to form C-3 (free base) or C-4 (salt form).

Conjugation reactions of laromustine and VNP4090CE occurred after incubation of laromustine or VNP4090CE with pooled HLM and co-factors NADPH, GSH, NAC, and CYS. Eight distinct conjugation reactions (M-1 to M-8) were identified and characterized by H-D, ¹³C-labeled laromustine, and MSⁿ experiments. M-4 and M-5 were further confirmed by NMR. The short-lived CH₃SO₂CH₂CH₂⁻, methylformamide and CH₃SO₂NHN=CHCH₂⁻ moieties were generated from laromustine. The reactive intermediates CH₃SO₂CH₂CH₂⁻ and methylformamide formed conjugates with GSH,

DMD # 69823

CYS, and NAC. The $\text{CH}_3\text{SO}_2\text{NHN}=\text{CHCH}_2-$ moiety formed conjugates with GSH and NAC. M-2, M-4 and M-6 were only detected from the incubation of laromustine because VNP4090CE does not contain a methylformamide group. All other conjugates were formed by both laromustine and VNP4090CE. Laromustine and VNP4090CE produced the same decomposition product-conjugates in buffer solution with or without HLM, which suggests that the decomposition of laromustine and VNP4090CE to active moieties does not involve P450 metabolism. These *in vitro* studies found that laromustine and VNP4090CE undergo activation via chemical decomposition in buffer solution in the presence or absence of HLM and with or without NADPH.

It is possible that these active moieties may alter cellular functions when they form conjugates with biomolecules. The degradation of laromustine produces methyl isocyanate (MIC), which is extremely toxic. MIC can induce damage by inhalation, ingestion, and contact in quantities as low as 0.4 ppm. Symptoms may include coughing, chest pain, dyspnea, asthma, irritation of the eyes, nose, and throat as well as skin damage. Higher levels of exposure, over 21 ppm, can result in pulmonary or lung edema, emphysema, and hemorrhaging, bronchial pneumonia, and death. Studies were conducted to evaluate both dose- and time-dependent ($N = 3$) response using N – succinimidyl N -methylcarbamate, a chemical entity that mimics the effects of methyl isocyanate *in vitro*. These studies demonstrated that isocyanates induce neutrophil apoptosis via activation of mitochondrial-mediated pathways along with reactive oxygen species production; depletion in antioxidant defense states; and elevated proinflammatory cytokine response (Mishra et al., 2008 and 2010; Ennever and Rosenkranz

DMD # 69823

1987; Bucher 1987). This study showed that laromustine produces several reactive intermediates that may play a role in toxicities seen in the clinical trials. Combined, these findings provide an understanding of both the beneficial and potentially harmful aspects of the metabolism of laromustine.

Acknowledgements

These studies were done at XenoTech, LLC (now Sekisui XenoTech, LLC), for Vion Pharmaceuticals Inc. We would like to thank Drs Paris B L, Haupt L, Ndikum-Moffor F, Campbell R, Usuki E, Skibbe J, Brobst D, Ogilvie B, and Parkinson A, for performing and supervising these studies.

Authorship Contributions

Participated in research design: AFN, IK

Wrote or contributed to writing of the manuscript: IV, AVW, AFN

References

"Alkylating Agents". (2014) US National Library of Medicine.
<http://livertox.nih.gov/AlkylatingAgents.htm>

Baillie TA (1992) Advances in the application of mass spectrometry to studies of drug metabolism, pharmacokinetics and toxicology. *Int. J. Mass Spectrom. Ion Proc.* 118/119, 289-314.

Baumann RP, Seow HA, Shyam K, Penketh PG, and Sartorelli AC (2005) The antineoplastic efficacy of the prodrug Cloretazine is produced by the synergistic interaction of carbamoylating and alkylating products of its activation. *Oncol Res* 15(6):313-25.

Brundrett RB, Cowens JW, Colvin M (1976), Chemistry of Nitrosoureas. Decomposition of Deuterated 1,3-Bis(2-chloroethyl)-1-nitrosourea. *Journal of Medicinal Chemistry*, Vol. 19, 7, 958-961

Bucher JR (1987) The toxicity of methyl isocyanate: Where do we stand? *Environ Health Perspect.* 72, 197-198

Buhl AE, Waldon DJ, Baker CA, and Johnson GA (1990) Minoxidil sulfate is the active metabolite that stimulates hair follicles. *J. Invest. Dermatol.* 95, 553-557

Colvid M, Cowens W, Brundrett RB, Kramer BS, Ludlum DB (1974).

DECOMPOSITION OF BCNU (1,3-BIS(2-CHLOROETHYL)-L-NITROSOUREA) IN AQUEOUS SOLUTION. *BIOCHEMICAL AND BIOPHYSICAL RESEARCH COMMUNICATIONS.* 60, 2, 515-520

DMD # 69823

- Ehrnebo M, Nilsson SO and Boreus LO (1979) Pharmacokinetics of ampicillin and its prodrugs bacampicillin and pivampicillin in man. *J Pharmacokinet Biopharm.*, 7, 429-451
- Ennever FK, and Rosenkranz HS (1987) Evaluating the potential for genotoxic carcinogenicity of methyl isocyanate. *Toxicol. Appl. Pharmacol.* 91 (3), 502 –505.
- Ensink JM, Vulto AG, van Miert AS, Tukker JJ, Winkel MB and Fluitman MA (1996) Oral bioavailability and in vitro stability of pivampicillin, bacampicillin, talampicillin, and ampicillin in horses. *Am J Vet Res.*, 57, 1021-1024
- Finch RA, Shyam K, Penketh PG, and Sartorelli AC (2001) 1,2-Bis(methylsulfonyl)-1-(2-chloroethyl)-2-(methylamino)-carbonylhydrazine (101M): A novel sulfonylhydrazine pro-drug with broad-spectrum antineoplastic activity. *Cancer Res* **61**:3033-3038.
- Giles F, Thomas D, Garcia-Manero G, Faderl S, Cortes J, Verstovsek S, Ferrajoli A, Jeha S, Beran M, Koller C, Andreeff M, Cahill A, Clairmont C, et. al. (2004) A phase I and pharmacokinetic study of VNP40101M, a novel sulfonylhydrazine alkylating agent, in patients with refractory leukemia. *Clin Cancer Res* **10**:2908-2917.
- Goodman LS, Wintrobe MM, Dameshek W, Goodman MJ, Gilman AZ, and McLennan MT (1946). "Nitrogen mustard therapy". *JAMA* 132 (3): 126–132.
- Kassahun K, Pearson PG, Tang W, McIntosh I, Leung K, Elmore C, Dean D, Wang R, Doss G, Baillie TA. (2001) Studies on the metabolism of troglitazone to reactive intermediates in vitro and in vivo; Evidence for novel biotransformation pathways

involving quinone methide formation and thiazolidinedione ring scission. *Chem. Res. Toxicol.* 14(1):62-70.

McLafferty FW and Turecek F (1993) "Interpretation of Mass Spectra" Chapter 4, Fourth Edition, *University Science Books*, 1993, page 51-83.

Mishra PK, Panwar H, Bhargava A, Gorantla VR, Jain SK, Banerjee S, and Maudar KK (2008) Isocyanates induces DNA damage, apoptosis, oxidative stress, and in inflammation in cultured human lymphocytes. *J. Biochem. Mol. Toxicol.* 22 (6), 429

Mishra PK, Khan S, Bhargava A, Panwar H, Banerjee S, Jain SK, and Maudar KK (2010) Regulation of isocyanate-induced apoptosis, oxidative stress, and in inflammation in cultured human neutrophils: isocyanate-induced neutrophils apoptosis. *Cell Biol. Toxicol.* 26 (3), 279

Mutlib AE, Strupczewski JT, and Chesson SM (1995) Application of hyphenated LC/NMR and LC/MS techniques in rapid identification of in vitro and in vivo metabolites of iloperidone. *Drug Metab Dispos* 23: 951–964.

Nassar AEF (2003a) Online hydrogen-deuterium exchange and a tandem quadrupole time-of-flight mass spectrometer coupled with liquid chromatography for metabolite identification in drug metabolism. *J. Chromatogr. Sci.*, 41, 398–404.

Nassar AEE and Adams PE (2003b) Metabolite characterization in drug discovery utilizing robotic liquid-handling, quadrupole time-of-flight mass spectrometry and in silico prediction. *Curr. Drug Metab.*, 4, 259–271.

Nassar AEF and Talaat R (2004) Strategies for dealing with metabolite elucidation in drug discovery and development. *Drug Discov. Today*, 9, 317–327.

DMD # 69823

- Nassar AE, King I, Paris B L, Haupt L, Ndikum-Moffor F, Campbell R, Usuki E, Skibbe J, Brobst D, Ogilvie B W, et al. (2009) An in vitro evaluation of the victim and perpetrator potential of the anti-cancer agent laromustine (VNP40101M), based on reaction phenotyping and inhibition and induction of cytochrome P450 (CYP) enzymes, *Drug Metab. Dispos.*; 37(9): 1922-1930.
- Nassar AE, Du J, Belcourt M, Lin X, King I, Lam T (2010a) "Case Study: Identification of *In Vitro* Metabolite/Decomposition Products of the Novel DNA Alkylating Agent Laromustine, Nassar, A-E. F.; Ed.; John Wiley & Sons, Chapter 6, "Biotransformation and metabolite elucidation of xenobiotics"
- Nassar AE, Du J, Belcourt M, Lin X, King I, and Lam T (2010b) "Case Study: The Unanticipated Loss of N₂ from Novel DNA Alkylating Agent Laromustine by Collision-Induced Dissociation: Novel Rearrangements, Nassar, A-E. F.; Ed.; John Wiley & Sons, Chapter 5, "Biotransformation and metabolite elucidation of xenobiotics"
- Nassar AE, King I and Du J (2010c). "In vitro profiling and mass balance of *the anti-cancer agent laromustine* [¹⁴C]-VNP40101M by rat, dog, monkey and human liver microsomes" *The Open Drug Metabolism Journal*, 4, 1-9
- Nassar AE, King I and Du J (2011) Characterization of Short-Lived Electrophilic Metabolites of the Anticancer Agent Laromustine (VNP40101M). *Chem. Res. Toxicol.*, 24 (4), pp 568–578
- Ortiz de Montellano PA (2013) Cytochrome P450-activated prodrugs. *Future Med Chem.*; 5(2): 213–228.

DMD # 69823

- Penketh PG, Shyam K, and Sartorelli AC (2000) Comparison of DNA lesions produced by tumor inhibitory 1,2-bis(sulfonyl)-hydrazines and chloroethylnitrosoureas. *Biochem Pharmacol* **59**:283-291.
- Penketh PG, Shyam K, Baumann RP, Remack JS, Brent TP, and Sartorelli AC (2004) 1,2-Bis(methylsulfonyl)-1-(2-chloroethyl)-2-[(methylamino)carbonyl]hydrazine (VNP40101M): I. Direct inhibition of O6-alkylguanine-DNA alkyltransferase (AGT) by electrophilic species generated by decomposition. *Cancer Chemother Pharmacol* **53**(4):279-87.
- Pochapsky SS and Pochapsky TC., 2001, Nuclear magnetic resonance as a tool in drug discovery, metabolism and disposition. *Curr Top Med Chem.*, 5, 427-41.
- Rautio J, Kumpulainen H, Heimbach T, Oliyai R, Dooman OH, Järvinen T, Savolainen J (2008) Prodrugs: design and clinical applications. *Nature Reviews Drug Discovery* **7**, 255-270
- Schiller GJ, O'Brien SM, Pigneux A, Deangelo DJ, Vey N, Kell J, Solomon S, Stuart RK, Karsten V, Cahill AL, et al. (2010) Single-agent laromustine, a novel alkylating agent, has significant activity in older patients with previously untreated poor-risk acute myeloid leukemia. *J Clin Oncol.* 10;28(5):815-21
- Scott RB (1970). "Cancer chemotherapy--the first twenty-five years". *Br Med J.* 4 (5730): 259–265
- Sjövall J, Magni L, and Bergan T (1978) Pharmacokinetics of Bacampicillin Compared with Those of Ampicillin, Pivampicillin, and Amoxycillin. *Antimicrob Agents Chemother.*, 13, 90–96

DMD # 69823

Watt AP, Mortishire-Smith RJ, Gerhard U, and Thomas SR, (2003) Metabolite identification in drug discovery. *Curr Opin Drug Discov Devel.* 1, 57-65.

Wiedemann GJ, Robins HI, Gutsche S, Mentzel M, Deeken M, Katschinski DM, Eleftheriadis S, Crahé R, Weiss C, and Storer B, Wagner T. (1996). "Ifosfamide, carboplatin and etoposide (ICE) combined with 41.8 degrees C whole body hyperthermia in patients with refractory sarcoma" *European Journal of Cancer* 32A (5): 888–92.

Footnote

Materials and Methods. For detailed information on these studies, please see the References (Nassar et al., 2009; Nassar et al., 2010a; Nassar et al., 2010b; Nassar et al., 2010c; and Nassar et al., 2011) and Supplementary Data.

In Memoriam to Dr. Alan C. Sartorelli. Alan C. Sartorelli, Ph.D was a professor of pharmacology for over 50 years at Yale School of Medicine, director of the Yale Comprehensive Cancer Center and chair of the Department of Pharmacology. His career highlights include receiving the Yale Comprehensive Cancer Center Lifetime Achievement Award in 2011, the Otto Kraymer Award in Pharmacology in 2002, the Experimental Therapeutics Award from the American Society of Pharmacology and Experimental Therapeutics, also in 2002, the Bruce F. Cain Memorial Award in 2001, and the Mike Hogg Award from the UTMD Anderson Cancer Center in 1989. Dr. Sartorelli authored and co-authored over 700 papers published in various scientific journals, and was the founding editor of *Pharmacology and Therapeutics*, and co-inventor on 16 U.S. patents for anti-cancer therapy. Laromustine is one of the compounds which was invented in his laboratory and has entered into advanced clinical trials.

Legends for Schemes and Figures:

Scheme 1. The pathway of activation of cyclophosphamide and ifosfamide

Scheme 2. Chemical structures of carmustine and lomustine and their degradation products

Figure 1. (a) Chemical structures of laromustine and VNP4090CE and (b) Chemical structure of laromustine and its metabolite/degradation products (Reproduced from Nassar et al., DMD, 2009)

Figure 2. Chromatograms from incubation of [¹⁴C]laromustine (100 μ M) with rat, dog, monkey, and human liver microsomes in the presence of NADPH (Reproduced from Nassar et al., DMD, 2009)

Figure 3. Correlation between the rate of formation of C-7 from [¹⁴C]laromustine (25 μ M) and CYP2B6 and CYP3A4/5 activity in a bank of human liver microsomes (n = 10) (Reproduced from Nassar et al., DMD, 2009)

Figure 4. FTMS results for MS/MS of m/z 325 peak using 9.4T Bruker Qe FTICR-MS, the same sample were injected three times to confirm the fragmentation ions. (Reproduced from Nassar et al., Chapter 5, "Biotransformation and metabolite elucidation of xenobiotics" 2010)

Figure 5. Proposed mechanism of formation fragmentation ions of m/z 251, 171, 143, 107, 81 and 63 (Reproduced from Nassar et al., Chapter 5, "Biotransformation and metabolite elucidation of xenobiotics" 2010)

Figure 6. Proposed fragmentation ions of laromustine of m/z 325, m/z 327 and m/z 330 (Reproduced from Nassar et al., Chapter 6, "Biotransformation and metabolite Elucidation of xenobiotics" 2010)

Figure 7. Proposed structure and fragmentation ions for C-7 (Reproduced from Nassar et al., Chapter 6, "Biotransformation and metabolite elucidation of xenobiotics" 2010)

Figure 8. Proposed formation mechanism of MW 214 (C-4 and C-5) (Reproduced from Nassar et al., Chapter 6, "Biotransformation and metabolite elucidation of xenobiotics" 2010)

Tables

Table 1: Formation of C-7 and loss of substrate in incubations of [¹⁴C]aromustine (25 and 100 μM) with various recombinant human CYP enzymes (25 pmol/incubation) expressed in *E. coli* (bactosomes)

Recombinant human CYP enzyme	Incubation time (min)	[¹⁴ C]aromustine (μM)	C-7 formed per incubation (pmol)	[¹⁴ C]aromustine detected per incubation (pmol)	Percent loss of substrate (%) ¹
Bactosome control	10	25	NC	5380	17.9%
Reductase control			NC	5390	17.7%
rCYP1A2			NC	5560	15.0%
rCYP2B6			376	5270	19.5%
rCYP2D6			NC	5470	16.5%
Bactosome control		100	NC	20100	14.7%
Reductase control			NC	20400	13.6%
rCYP1A2			NC	20300	13.9%
rCYP2B6			513	20000	15.3%
rCYP2D6			NC	20100	14.6%

1: Percent loss of substrate was determined based on the zero-minute microsomal sample.
 NC: Not calculated (represents a zero or negative value beyond the AUC level)
 Pmol values are the mean of duplicate determinations and are rounded to three significant figures.
 Percent values are rounded to one decimal place. Reproduced from Nassar et al., DMD, 2009.

DMD # 69823

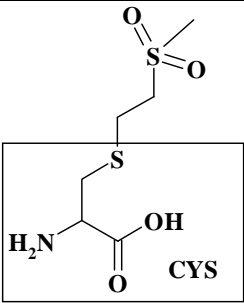
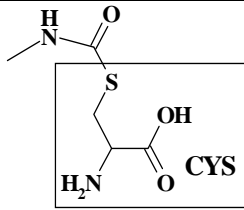
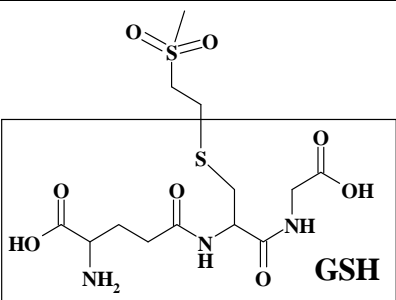
Nominal mass	Experimental			Average mass, <i>m/z</i>	Formula	error, ppm
	Trial 1, <i>m/z</i>	Trial 2, <i>m/z</i>	Trial 3, <i>m/z</i>			
325	325.0408	325.0407	325.0405	325.0407	C ₆ H ₁₈ CIN ₄ O ₅ S ₂	-1.64
308	308.0141	308.0140	308.0140	308.0141	C ₆ H ₁₅ CIN ₃ O ₅ S ₂	-1.57
251	250.9923	250.9924	250.9923	250.9923	C ₄ H ₁₂ CIN ₂ O ₄ S ₂	-0.58
143	142.9925	142.9926	142.9926	142.9925	C ₃ H ₈ CIO ₂ S	2.12
107	107.0161	107.0161	107.0160	107.0161	C ₃ H ₇ O ₂ S	0.25
93	93.0214	93.0214	93.0214	93.0214	C ₂ H ₆ CIN ₂	0.03

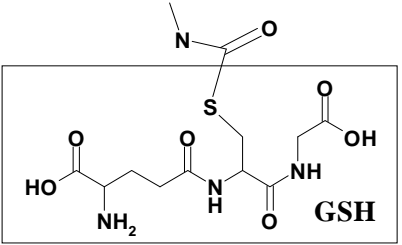
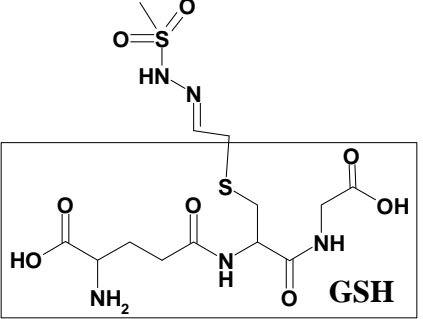
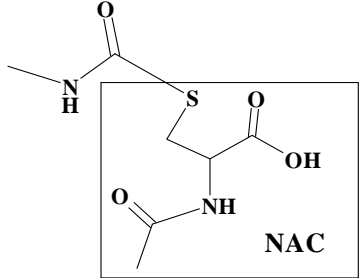
Reproduced from Nassar et al., Chapter 5, "Biotransformation and metabolite elucidation of Xenobiotics" 2010

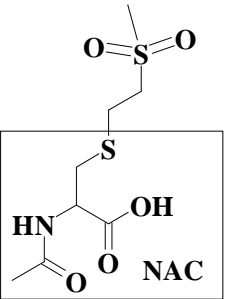
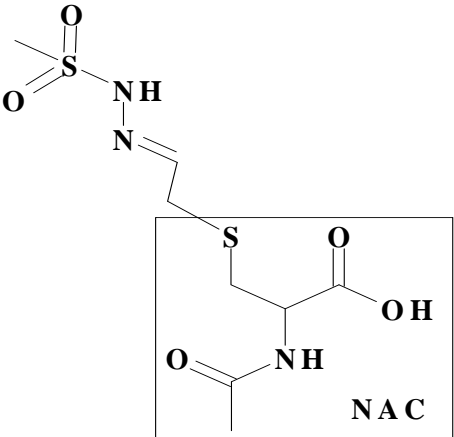
Component (C) Molecular formula	MW, amu		RT, min	N-rule*		RDBE**		H-D***	
	¹² C	¹³ C ₂		Expected	Observed	Expected	Observed	Expected	Observed
C-1 C ₃ H ₈ O ₃ S	124.2	126.2	5.5	Even or no	no	0	0	1	1
C-3 C ₄ H ₁₀ N ₂ O ₄ S ₂	214.3	216.3	9.3	Even or no	Even	1	1	1	1
C-4a**** C ₂ H ₅ ClO	80.5	ND	11.5	Even or no	ND	0	ND	1	ND
C-4 C ₄ H ₁₀ N ₂ O ₄ S ₂	214.3	216.3	11.5	Even or no	Even	1	1	1	1
C-5 C ₄ H ₁₀ N ₂ O ₄ S ₂	214.3	216.3	19.5	Even or no	Even	1	1	0	0
C-7 C ₆ H ₁₄ CIN ₃ O ₆ S ₂	323.8	325.8	36.0	Odd	Odd	1	1	2	2
C-8 (VNP4090CE, 90CE) C ₄ H ₁₁ CIN ₂ O ₄ S ₂	250.7	252.7	38.1	Even or no	Even	0	0	1	1
Parent Drug (laromustine) C ₆ H ₁₄ CIN ₃ O ₅ S ₂	307.8	309.8	43.0	Odd	Odd	1	1	1	1

MW= Molecular-Weight
¹³C₂= stable isotope (¹³C-labeled laromustine)
 *=If a compound has an odd mass it definitely has a N atom in its structure, and contains an odd number of N atoms (1, 3, 5 etc.). If a compound has an even mass, it has either no N or an even number of N atoms in its structure (0, 2, 4 etc.).
 **=Ring Double Bond Equivalent (RDBE)
 ***= the number of labile protons on the molecule
 ****=[¹⁴C]2-chloroethanol peak (C-4a) overlaps with the component C-4; 2-chloroethanol peak was detected by GC-MS
 ND=No Data available from LC-MS
 Reproduced from Nassar et al., Chapter 6, "Biotransformation and metabolite elucidation of xenobiotics" 2010

Table 4: *In vitro* conjugation reactions of laromustine and VNP4090CE

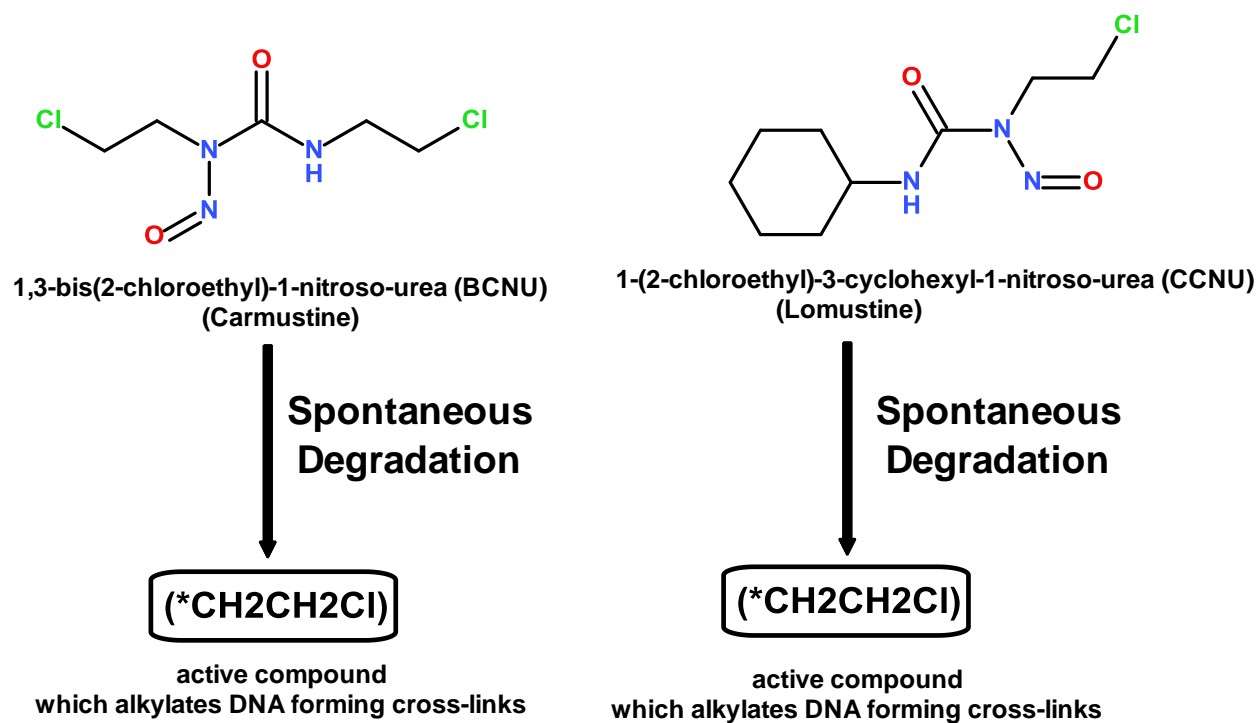
Compound - No.	Proposed Structure	MW, amu		RT*, min	H-D**		N-rule***		RDBE****	
		¹² C	¹³ C		Expected	Observed	Expected	Observed	Expected	Observed
M-1		227.3	229.3	17.5	3	3	Odd	Odd	1	1
M-2		178.2	178.2	20.2	4	4	No or Even	Even	2	2
M-3		413.5	415.5	27.6	6	6	Odd	Odd	4	4

M-4		364.4	364.4	27.8	7	7	No or Even	Even	5	5
M-5		441.5	443.5	33.4	7	7	Odd	Odd	5	5
M-6		220.3	220.3	37.7	3	3	No or Even	Even	3	3

M-7		269.3	271.3	43.0	2	2	Odd	Odd	2	2
M-8		297.4	299.4	46.5	3	3	Odd	Odd	3	3

MW= Molecular-Weight, *=approximate retention time on LC-MS, **= the number of labile protons on the molecule; the protonating species in the H-D experiments is D and not H, ***=if a compound has an odd mass it has an N atom in its structure, and contains an odd number of N atoms (1, 3, 5 etc.). If a compound has an even mass, it has either no N or an even number of N atoms in its structure (0, 2, 4 etc.); the nitrogen rule only applies to unprotonated, intact molecules, ****=Ring Double Bond Equivalents (RDBE), sulfone oxygen atoms (i.e., those double-bonded to sulfur) do not count toward rings and double bonds, ¹³C=[chloroethyl-1,2], Reproduced from Nassar et al., Chem. Res. Toxicol, 2011

Scheme 1



Scheme 2

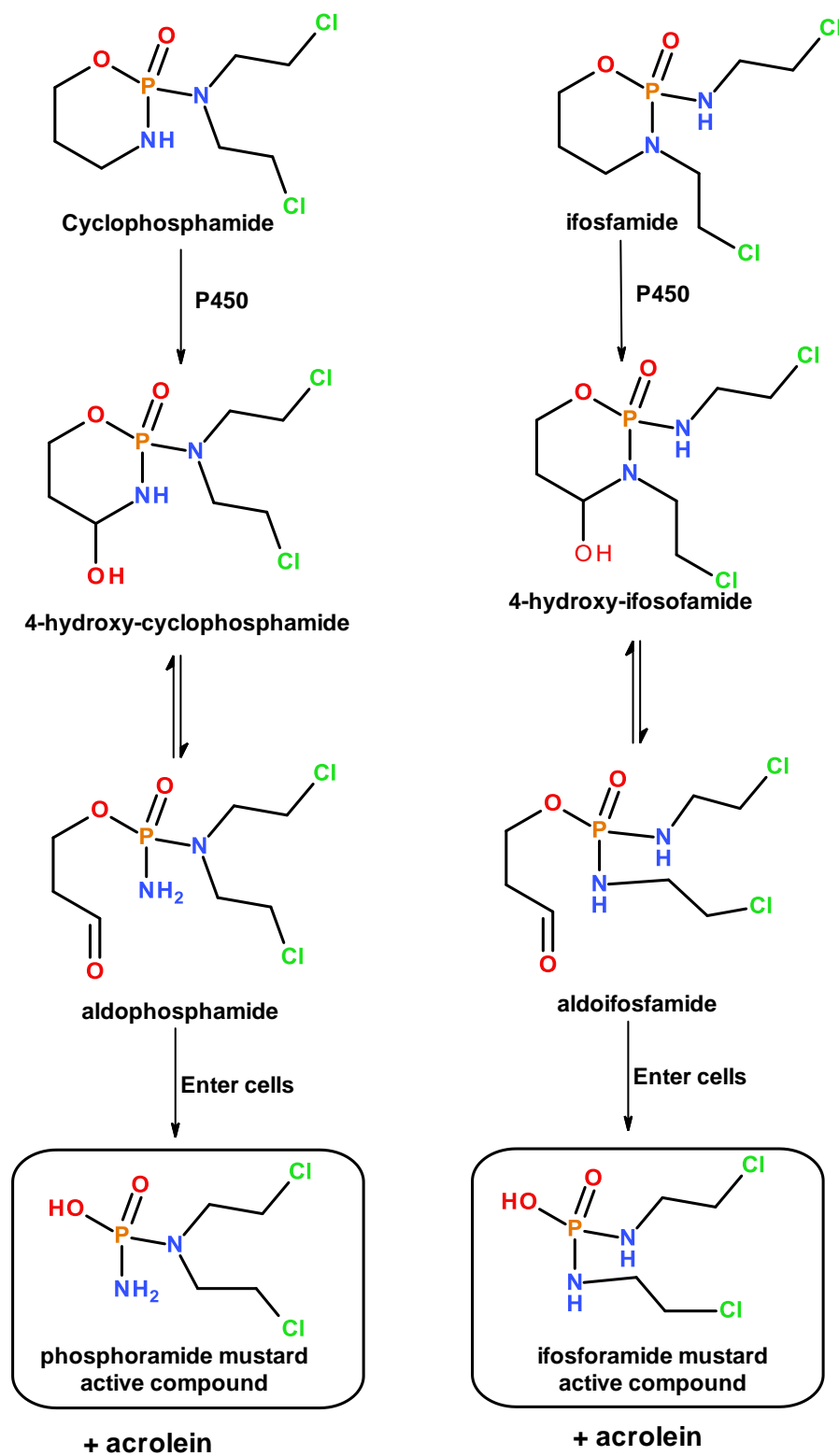


Fig. 1a

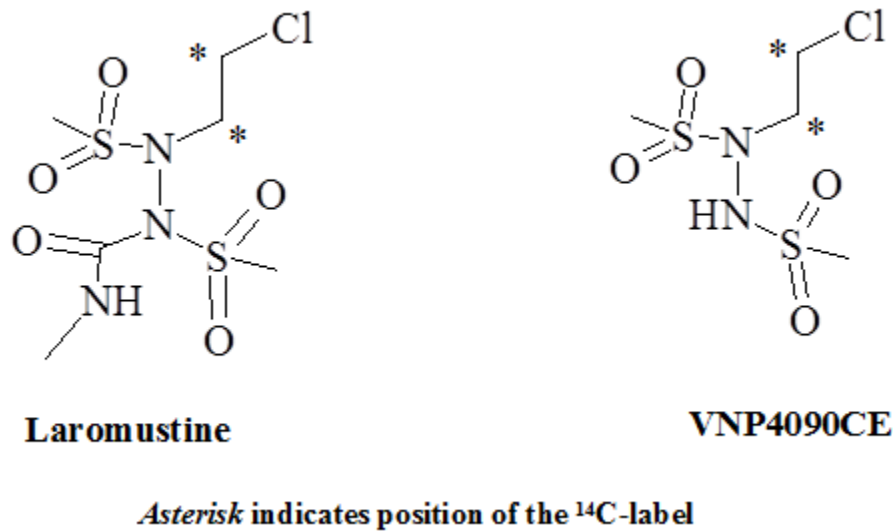


Fig. 1b

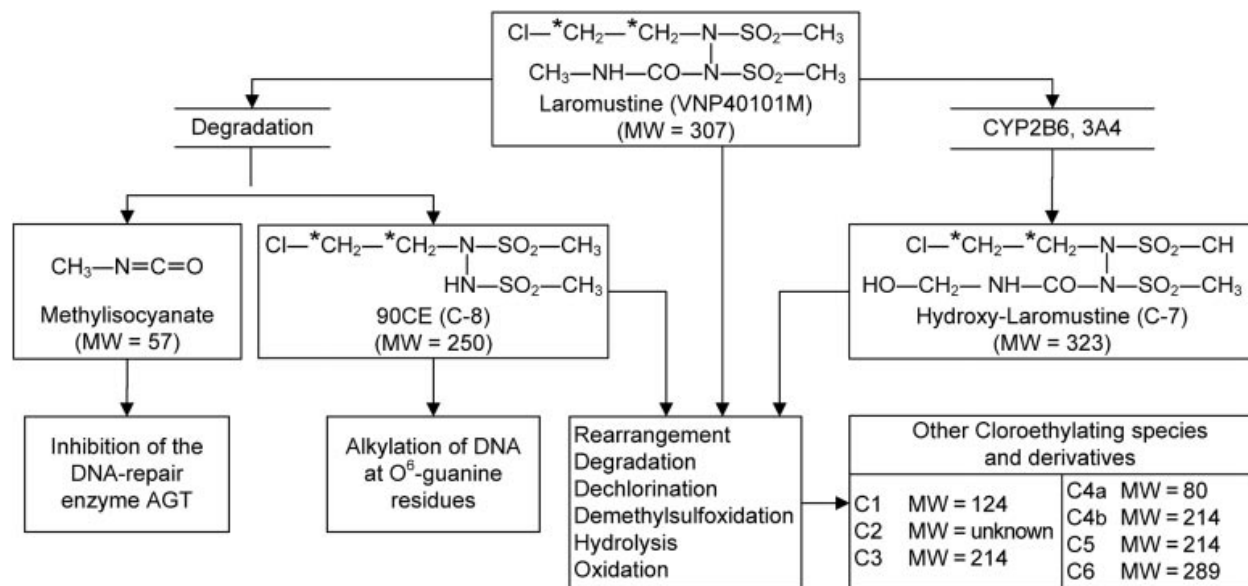


Fig. 2

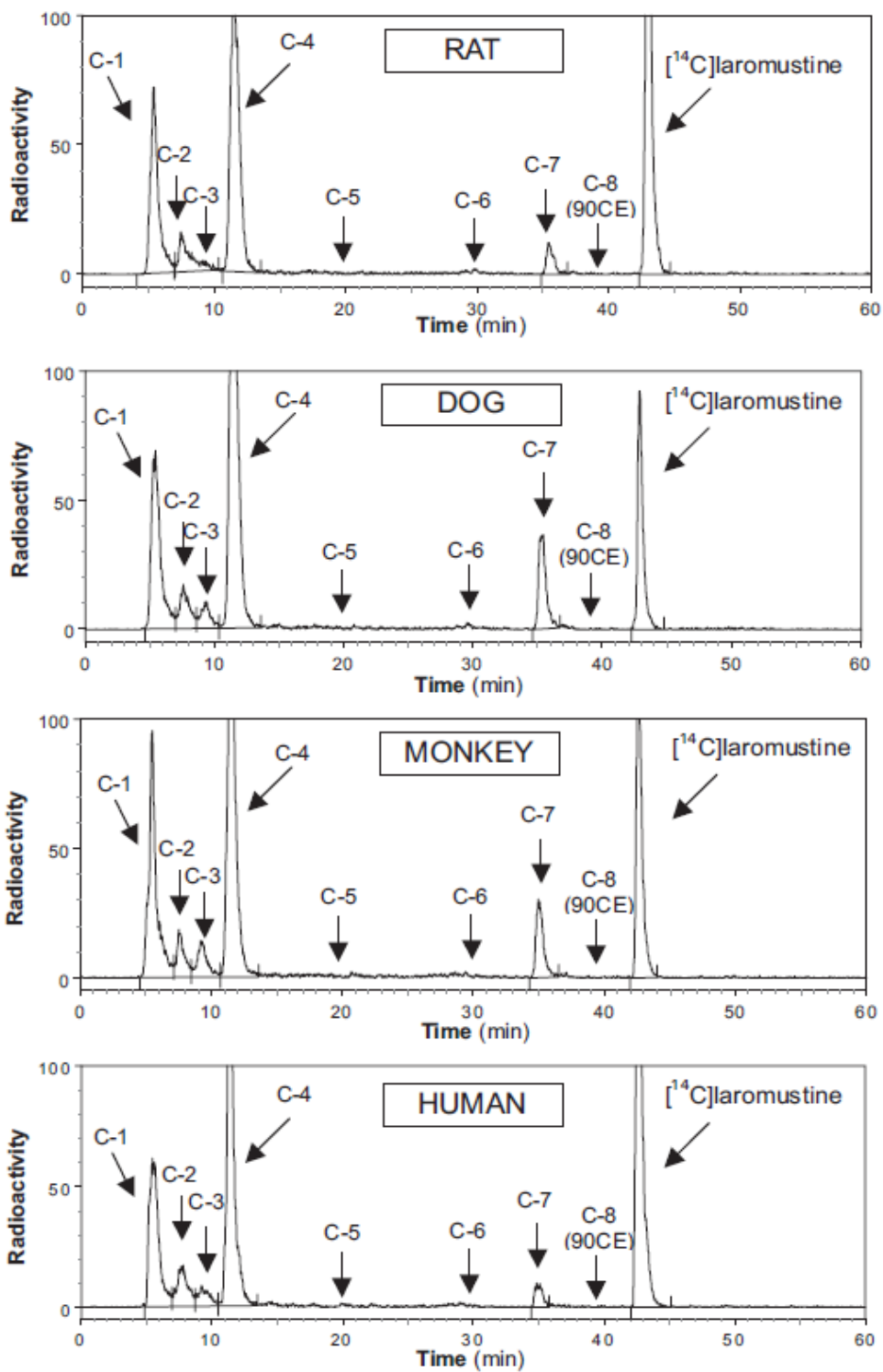


Fig. 3

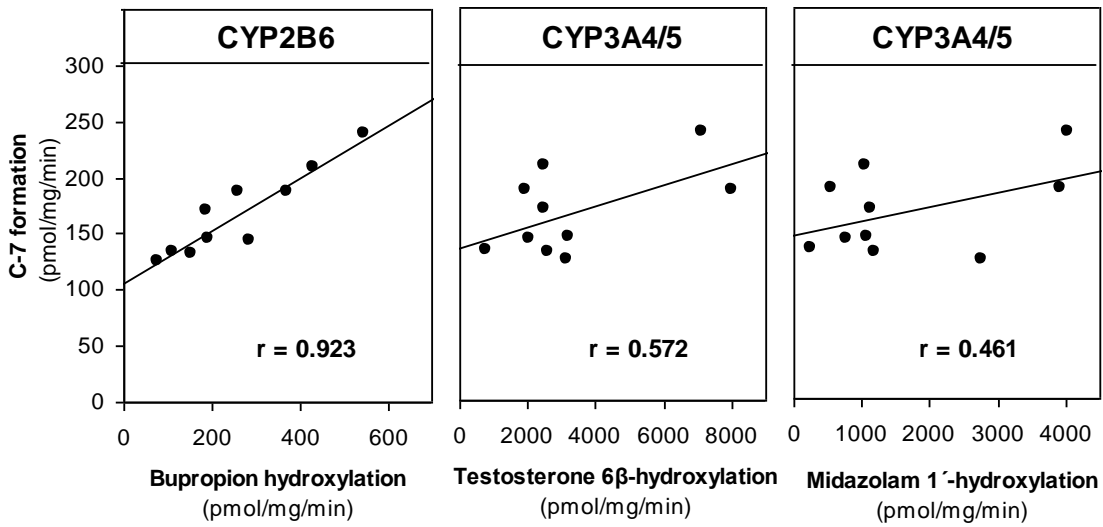


Fig. 5.

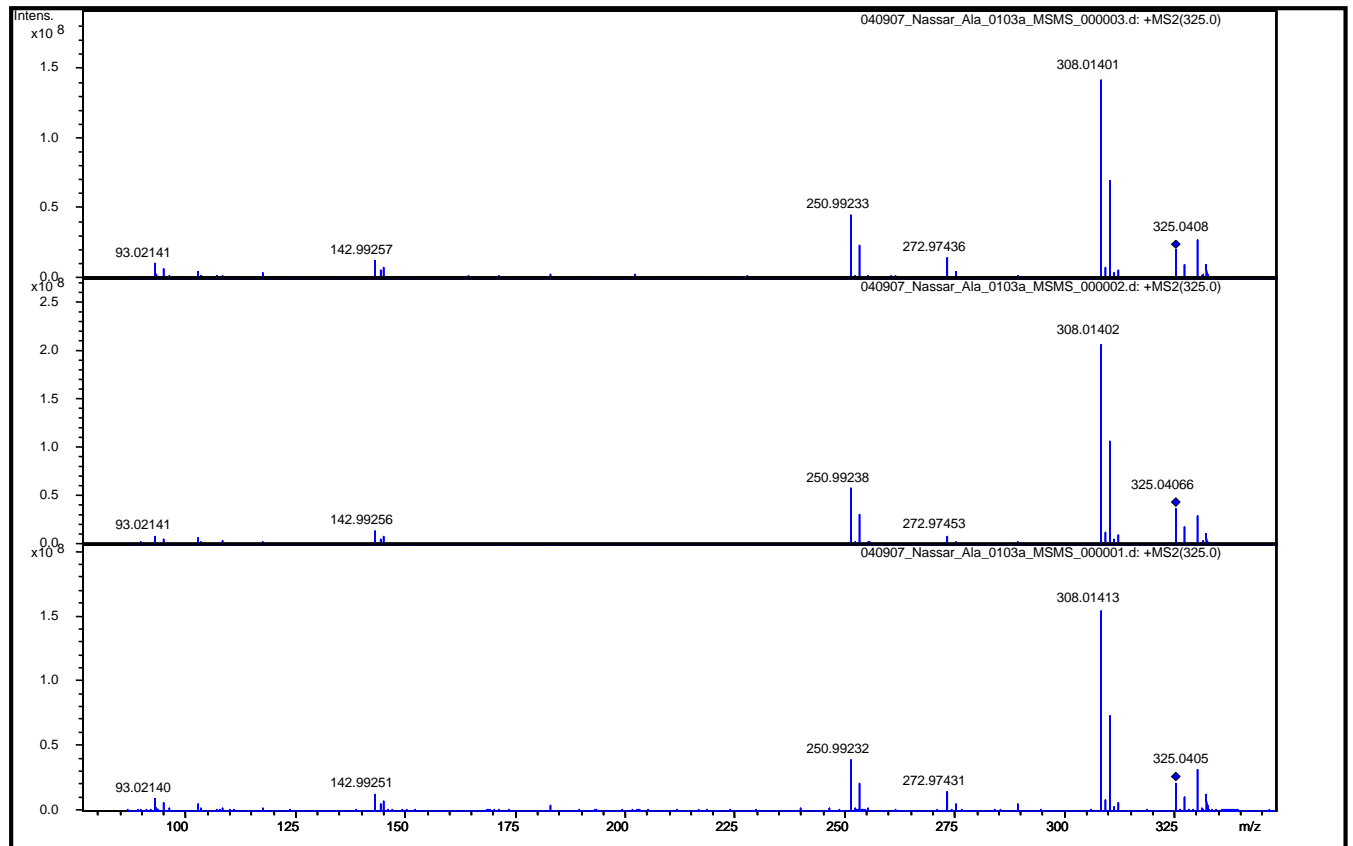


Fig. 6

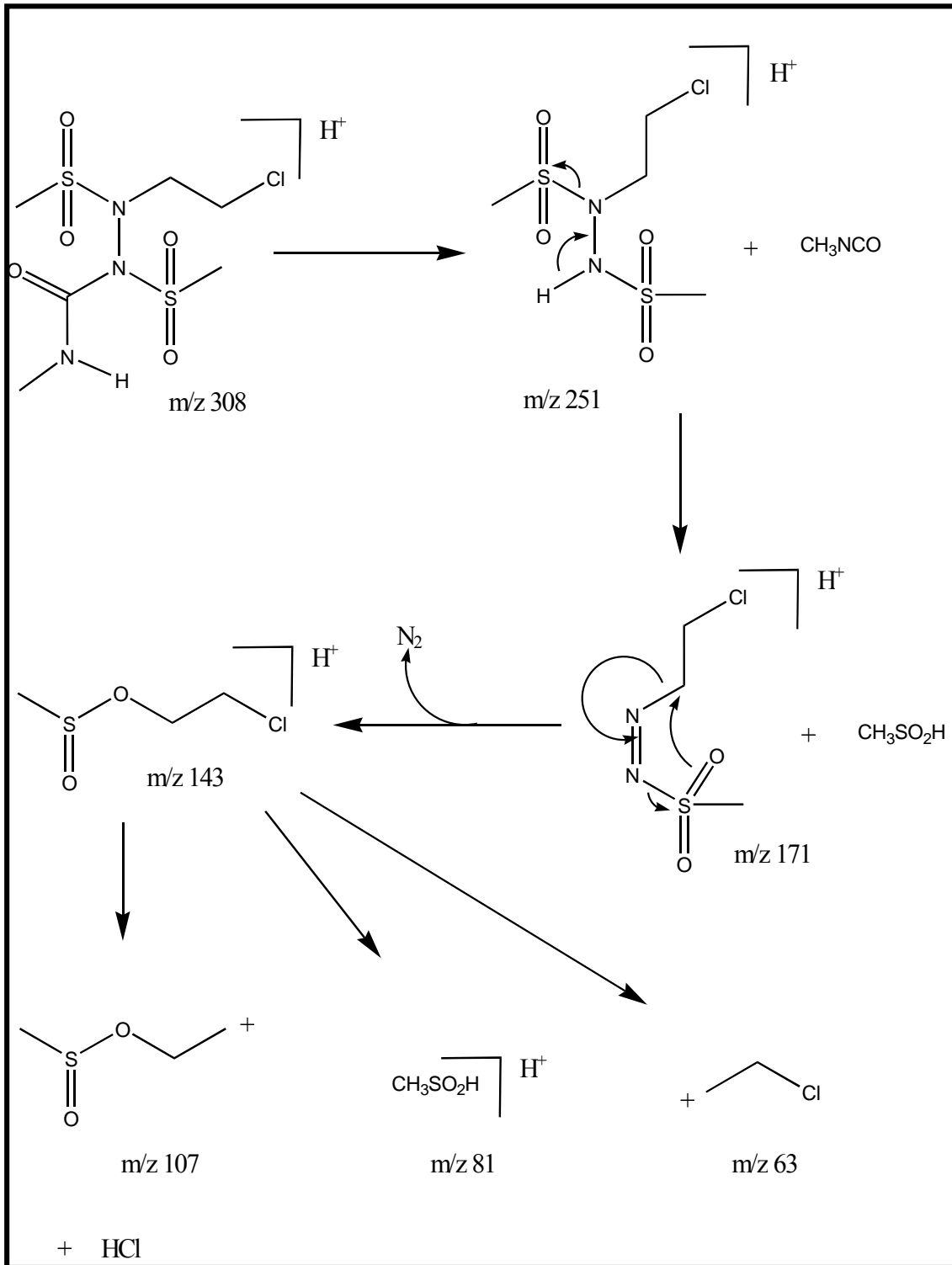


Fig. 7

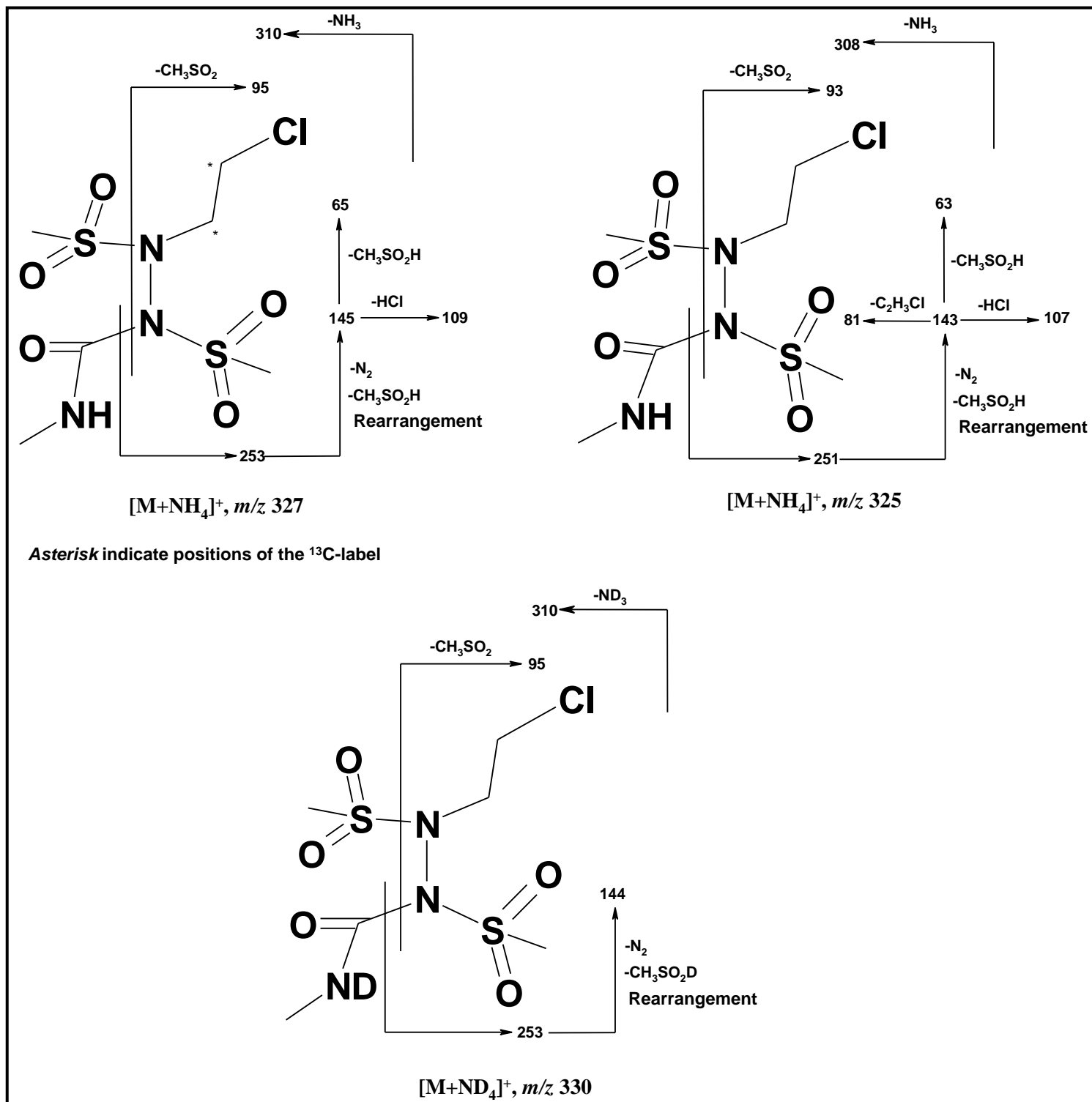


Fig. 8

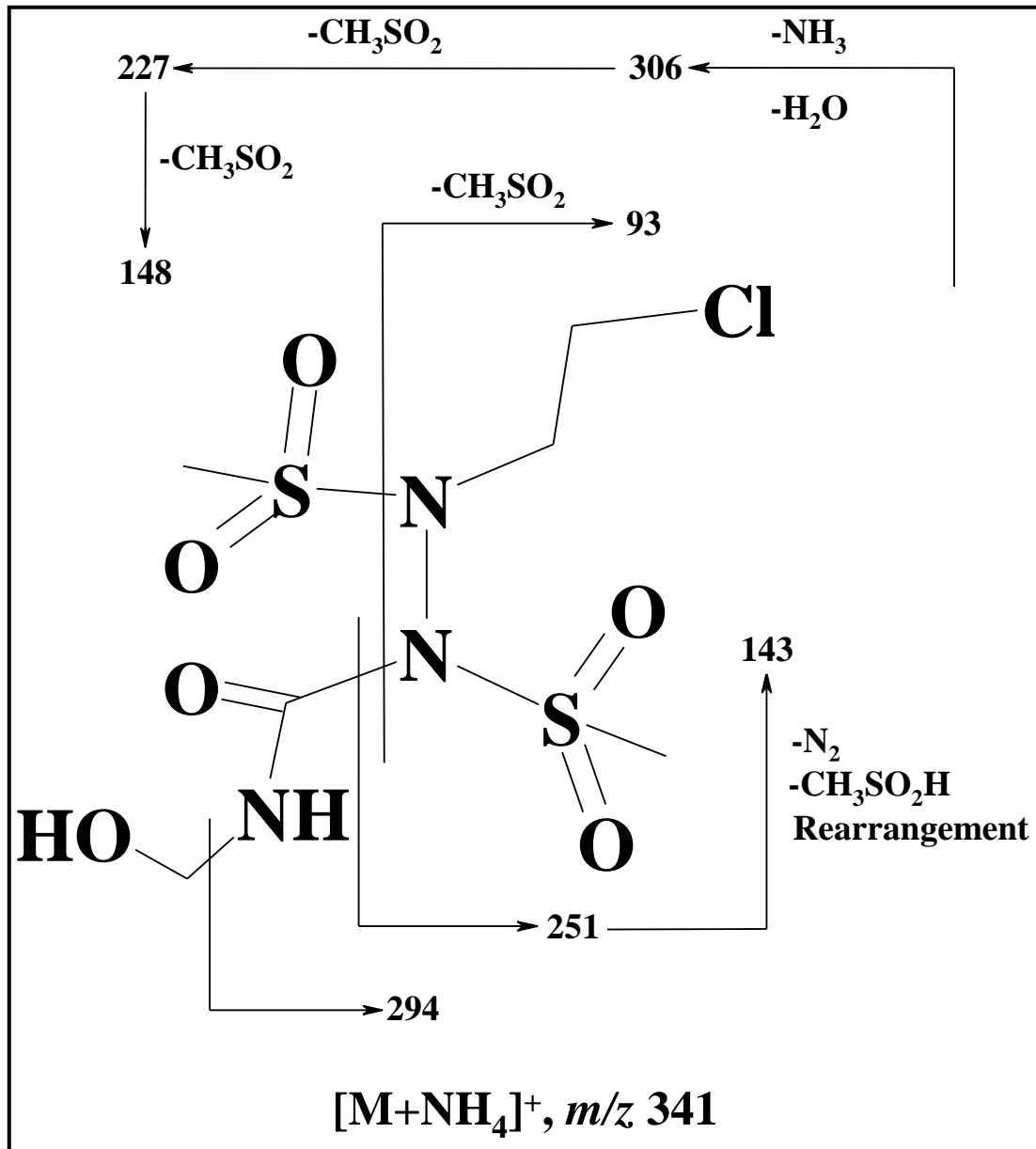
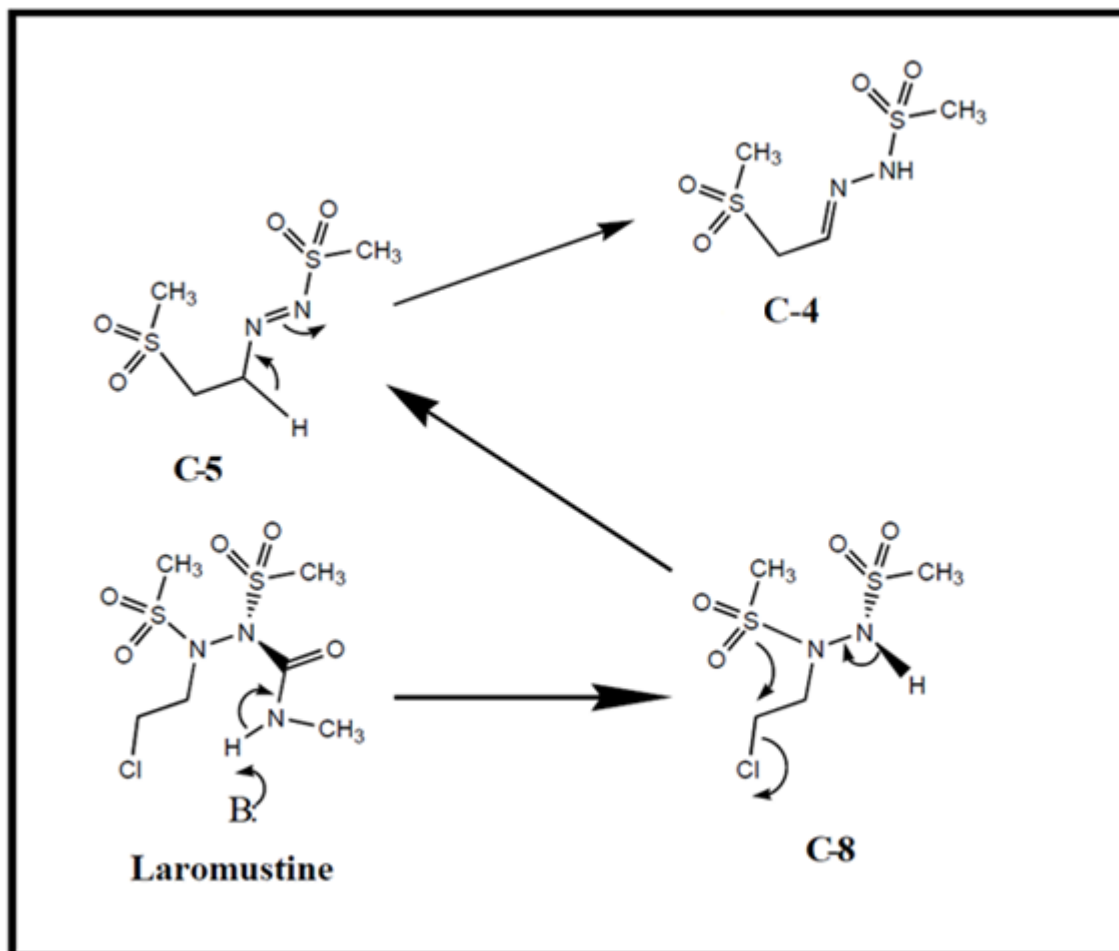


Fig. 9



DMD Manuscript #69823

Biotransformations and Rearrangement of Laromustine

Ala F. Nassar, Adam V. Wisnewski, Ivan King

School of Medicine, Department of Internal Medicine, Yale University, New Haven, CT,

Department of Chemistry, 55 N. Eagleville Rd., University of Connecticut, Storrs, CT,

Metastagen, Inc., Wilmington, DE, United States.

Table legends

1. Percent recovery of [¹⁴C]laromustine from incubations with rat, dog, monkey and human liver microsomes (1 mg protein/mL) in the presence and absence of NADPH
2. Conversion of [¹⁴C]laromustine (100 μM) to radioactive components (C-1, C-2, C-3, C-4 and C-7) by rat, dog, monkey and human liver microsomes (1 mg protein/mL) in the presence and absence of NADPH
3. Percent conversion of [¹⁴C]laromustine (100 μM) to radioactive components (C-1, C-2, C-3, C-4 and C-7) by rat, dog, monkey and human liver microsomes (1 mg protein/mL) in the presence and absence of NADPH
4. Formation of C-7 and loss of substrate in incubations of [¹⁴C]laromustine (25 and 100 μM) with various recombinant human CYP enzymes (25 pmol/incubation) expressed in insect cells (supersomes)
5. Analysis of the correlation between the rate of formation of C-7 from [¹⁴C]laromustine (25 μM) and marker CYP and FMO activities in a bank of human liver microsomes (n = 10)
6. Individual and Mean Plasma Concentrations and Pharmacokinetics of Total Radioactivity Following Intravenous Bolus Dose Administration of 10 mg/kg [¹⁴C]laromustine to Group 3 Rats
7. Reactive moieties originating from laromustine and VNP4090CE

Figure legends

1. LC-MS spectrum of $[M+NH_4]^+$, m/z 325, laromustine in LTQ (A) Full scan, (B) MS2, (C) MS3, (D) MS4 and (E) MS5 (Reproduced from Nassar et al., Chapter 5, "Biotransformation and metabolite elucidation of xenobiotics" 2010)
2. Representative LC-MS spectra of $[M+NH_4]^+$, m/z 232, C-3 (A) Full Scan, (B) MS2 and (C) MS3 (Reproduced from Nassar et al., Chapter 6, "Biotransformation and metabolite Elucidation of xenobiotics" 2010)
3. Representative LC-MS spectra of $[M+NH_4]^+$, m/z 232, C-4 (A) Full Scan, (B) MS2 and (C) MS3 (Reproduced from Nassar et al., Chapter 6, "Biotransformation and metabolite Elucidation of xenobiotics" 2010)
4. Proposed structure and fragmentation ions for C-4 (Reproduced from Nassar et al., Chapter 6, "Biotransformation and metabolite Elucidation of xenobiotics" 2010)
5. Proposed structure and fragmentation ions for C-5 (Reproduced from Nassar et al., Chapter 6, "Biotransformation and metabolite Elucidation of xenobiotics" 2010)
6. LC-MS spectra of m/z 414, M-3 (A) full scan MS, (B) MS2, (C) MS3, (D) MS4, and (E) MS5 (Reproduced from Nassar et al., Chem. Res. Toxicol, 2011)
7. Proposed structure and fragmentation pattern for M-3 (Reproduced from Nassar et al., Chem. Res. Toxicol, 2011)

Table 1s: Percent recovery of [¹⁴C]Iaromustine from incubations with rat, dog, monkey and human liver microsomes (1 mg protein/mL) in the presence and absence of NADPH

Species	Cofactor (NADPH)	Incubation time (min)	Supernatant percent recovery	Pellet percent recovery	Total percent recovery for supernatant and pellet
Rat	+	0	98.6%	9.0%	107.6%
		60	95.1%	11.6%	106.7%
	-	0	99.9%	9.5%	109.4%
		60	91.6%	12.2%	103.7%
Dog	+	0	99.5%	9.3%	108.8%
		60	93.8%	11.2%	105.0%
	-	0	97.8%	10.1%	107.9%
		60	90.8%	11.6%	102.4%
Monkey	+	0	98.6%	9.4%	108.0%
		60	94.0%	11.2%	105.2%
	-	0	99.6%	9.1%	108.7%
		60	91.7%	12.2%	103.9%
Human	+	0	97.8%	9.8%	107.6%
		60	97.8%	12.0%	109.8%
	-	0	97.2%	9.7%	106.9%
		60	92.1%	12.4%	104.5%

+ NADPH present, - NADPH absent

Recovery determined by liquid scintillation counting.

Percentages are the mean of duplicate determinations and are rounded to one decimal place.

Reproduced from Nassar et al., The Open Drug Metabolism Journal, 2010

Table 2s: Conversion of [¹⁴C]Iaromustine (100 μM) to radioactive components (C-1, C-2, C-3, C-4 and C-7) by rat, dog, monkey and human liver microsomes (1 mg protein/mL) in the presence and absence of NADPH

Species	Cofactor (NADPH)	Incubation time (min)	C-1 formed per incubation (pmol) ¹	C-2 formed per incubation (pmol) ¹	C-3 formed per incubation (pmol) ¹	C-4 formed per incubation (pmol) ¹	C-7 formed per incubation (pmol) ¹	Mean substrate per incubation (pmol)	Total pmol per incubation	Percent loss of substrate (%)	Mass balance
Rat	+	0	NC	NC	NC	NC	NC	54300	54300	NA	100.0
		60	9770	2320	NC	17300	199	20100	49600	63.0	91.4
	-	0	NC	NC	NC	NC	NC	50700	50700	NA	100.0
		60	10600	2370	NC	17000	NC	21000	50900	58.6	100.6
Dog	+	0	NC	NC	NC	NC	NC	51900	51900	NA	100.0
		60	11500	2590	1640	22400	4070	9370	51500	81.9	99.3
	-	0	NC	NC	NC	NC	NC	53900	53900	NA	100.0
		60	11600	2640	861	22200	NC	25400	62700	52.8	116.4
Monkey	+	0	NC	NC	NC	NC	NC	56800	56800	NA	100.0
		60	12200	2290	2250	20800	2430	13700	53600	75.9	94.3
	-	0	NC	NC	NC	NC	NC	55500	55500	NA	100.0
		60	12200	2620	1520	20500	NC	21600	58400	61.1	105.2
Human	+	0	NC	NC	NC	NC	NC	62400	62400	NA	100.0
		60	10200	3100	1410	19200	171	22700	56800	63.7	91.0
	-	0	NC	NC	NC	NC	NC	56500	56500	NA	100.0
		60	10900	2700	1350	21200	NC	23300	59400	58.7	105.3

+ NADPH present, - NADPH absent, NA: Not applicable, NC: Not calculated (represents a zero or negative value beyond the AUC level)

¹: Values have been blank-corrected with appropriate zero-time sample.

Values are the mean of duplicate determinations.

Values are rounded to three significant figures. Percentages are rounded to one decimal place.

Mass balance = Total pmol ÷ Total pmol at zero-time x 100%

Lower limit of quantitation was 0.25 μM (2.5 pmol per injection). Reproduced from Nassar et al., The Open Drug Metabolism Journal, 2010

Table 3s: Percent conversion of [¹⁴C]Iaromustine (100 μM) to radioactive components (C-1, C-2, C-3, C-4 and C-7) by rat, dog, monkey and human liver microsomes (1 mg protein/mL) in the presence and absence of NADPH

Species	Cofactor (NADPH)	Incubation time (min)	Percent C-1 formation (%)	Percent C-2 formation (%)	Percent C-3 formation (%)	Percent C-4 formation (%)	Percent C-7 formation (%)	Total Formation (%)	Percent loss of substrate (%)
Rat	+	0	NC	NC	NC	NC	NC	NC	NA
		60	18.0	4.3	NC	31.8	0.4	54.4	63.0
	-	0	NC	NC	NC	NC	NC	NC	NA
		60	20.9	4.7	NC	33.7	NC	59.2	58.6
Dog	+	0	NC	NC	NC	NC	NC	NC	NA
		60	22.2	5.0	3.2	43.1	7.8	81.2	81.9
	-	0	NC	NC	NC	NC	NC	NC	NA
		60	21.5	4.9	1.6	41.2	NC	69.2	52.8
Monkey	+	0	NC	NC	NC	NC	NC	NC	NA
		60	21.4	4.0	4.0	36.5	4.3	70.2	75.9
	-	0	NC	NC	NC	NC	NC	NC	NA
		60	21.9	4.7	2.7	37.0	NC	66.4	61.1
Human	+	0	NC	NC	NC	NC	NC	NC	NA
		60	16.4	5.0	2.3	30.8	0.3	54.6	63.7
	-	0	NC	NC	NC	NC	NC	NC	NA
		60	19.4	4.8	2.4	37.5	NC	64.0	58.7

+ NADPH present, - NADPH absent

Values have been blank-corrected with appropriate zero-time sample.

Values are the mean of duplicate determinations.

Values and percentages are rounded to one decimal place.

NA: Not applicable, NC: Not calculated (represents a zero or negative value beyond the AUC level)

Percent Formation (%) = (Formation per Incubation (pmol) ÷ Mean Substrate per Incubation (pmol) at zero-time) x 100%

Total formation (%) = Sum of Percent Formation values, Reproduced from Nassar et al., The Open Drug Metabolism Journal, 2010

Table 4s: Formation of C-7 and loss of substrate in incubations of [¹⁴C]laromustine (25 and 100 μM) with various recombinant human CYP enzymes (25 pmol/incubation) expressed in insect cells (supersomes)

Recombinant human CYP enzyme	Incubation time (min)	[¹⁴ C]laromustine (μM)	C-7 formed per incubation (pmol)	[¹⁴ C]laromustine detected per incubation (pmol)	Percent loss of substrate (%) ¹	
Insect cell control	10	25	NC	5440	17.0%	
rCYP2A6 + b ₅ ²			NC	6490 ²	8.0% ²	
rCYP2C8 + b ₅			NC	5440	16.9%	
rCYP2C9 + b ₅			NC	5470	16.5%	
rCYP2C19 + b ₅			NC	5390	17.6%	
rCYP3A4 + b ₅			362	5150	21.3%	
Insect cell control		100	100	NC	20100	14.6%
rCYP2C8 + b ₅				NC	19600	16.8%
rCYP2A6 + b ₅ ²				NC	21600 ²	7.4% ²
rCYP2C9 + b ₅				NC	19900	15.6%
rCYP2C19 + b ₅	NC			19400	17.5%	
rCYP3A4 + b ₅			549	18700	20.4%	

1: Percent loss of substrate was determined based on the zero-minute microsomal sample.

2: rCYP2A6 incubations were performed as a separate experiment.

NC: Not calculated (represents a zero or negative value beyond the AUC level)

Pmol values are the mean of duplicate determinations and are rounded to three significant figures.

Percent values are rounded to one decimal place with the exception of values at or above 100% which are rounded to three significant figures. Reproduced from Nassar et al., The Open Drug Metabolism Journal, 2010

Table 5s: Analysis of the correlation between the rate of formation of C-7 from [¹⁴C]laromustine (25 μM) and marker CYP and FMO activities in a bank of human liver microsomes (n = 10)

Activity/enzyme		C-7 correlation coefficient
Phenacetin O-dealkylase	CYP1A2	-0.0698
Coumarin 7-hydroxylase	CYP2A6	0.678 ¹
Bupropion hydroxylase	CYP2B6	0.923
Paclitaxel 6α-hydroxylase	CYP2C8	0.452
Diclofenac 4'-hydroxylase	CYP2C9	-0.343
S-Mephenytoin 4'-hydroxylase	CYP2C19	-0.0231
Dextromethorphan O-demethylase	CYP2D6	0.691 ¹
Chlorzoxazone 6-hydroxylase	CYP2E1	-0.442
Testosterone 6β-hydroxylase	CYP3A4/5	0.572
Midazolam 1'-hydroxylase	CYP3A4/5	0.461
Lauric acid 12-hydroxylase	CYP4A11	0.137
Benzydamine N-oxidation	FMO	-0.113

¹The moderate correlation observed may be artifact due to the enzyme to enzyme correlation with CYP2B6 activity among the individual microsomal samples (*i.e.*, $r = 0.598$ and $r = 0.401$).

Samples from 16 individuals were evaluated but only data from 10 individuals were used in the data processing. The highest correlation coefficient is bold. Reproduced from Nassar et al., *The Open Drug Metabolism Journal*, 2010

Table 6s. Individual and Mean Plasma Concentrations and Pharmacokinetics of Total Radioactivity Following Intravenous Bolus Dose Administration of 10 mg/kg [¹⁴C]Iaromustine to Group 3 Rats (Reproduced from Nassar et al., Xenobiotica, 2015)

Time	Plasma μg Equivalents/mL				Mean	SD
	Rat 9A	Rat 10A	Rat 11A	Rat 12A		
0	BQL	BQL	BQL	BQL	0.000	0.000
0.083	8.973	9.000	8.126	7.310	8.352	0.805
0.25	6.935	7.479	6.999	6.169	6.896	0.542
0.5	6.297	5.855	5.837	5.366	5.839	0.380
1	4.599	4.358	4.084	3.614	4.164	0.423
2	3.766	3.758	3.561	3.136	3.555	0.295
4	3.177	2.974	2.905	2.486	2.886	0.290
7	3.013	2.536	2.721	2.357	2.657	0.280
10	2.530	2.392	2.169	1.971	2.266	0.246
24	2.093	1.831	1.969	1.490	1.846	0.260
48	1.479	1.470	1.445	1.237	1.408	0.115
C_{max} (μg equivalents/mL)	8.973	9.000	8.126	7.310	8.352	0.805
$t_{1/2}$ (min)	48.9	76.1	63.4	58.9	61.8	11.3
AUC_{0-48} ($\text{h} \cdot \mu\text{g}/\text{mL}$)	110.029	104.829	101.681	84.820	100.340	10.904
$\text{AUC}_{0-\text{Inf}}$ ($\text{h} \cdot \mu\text{g}/\text{mL}$)	214.444	295.830	233.922	189.906	233.526	45.272

BQL = 0.065 μg Equivalents/mL; treated as zero for mean and SD calculations

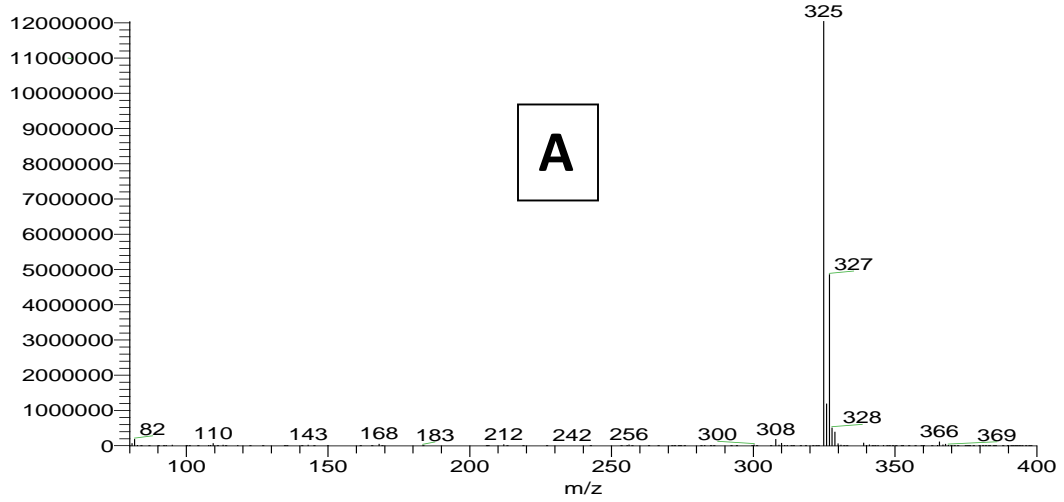
Table 7s: Reactive moieties originating from laromustine and VNP4090CE					
Moiety		Moiety originating from	Conjugate product		
Chemical structure	MW, amu		GSH	NAC	CYS
CH₃SO₂CH₂CH₂-	107	VNP4090CE	M-3	M-7	M-1
		laromustine	M-3	M-7	M-1
CH₃NHCO-	58	VNP4090CE	ND	ND	ND
		laromustine	M-4	M-6	M-2
CH₃SO₂NHN=CHCH₂-	135	VNP4090CE	M-5	M-8	ND
		laromustine	M-5	M-8	ND

ND = not detected, MW= Molecular-Weight, Reproduced from Nassar et al., Chem. Res. Toxicol, 2011

Figure 1s: LC-MS spectrum of [M+NH4]⁺, m/z 325, laromustine in LTQ (A) Full scan, (B) MS², (C) MS³, (D) MS⁴ and (E) MS⁵

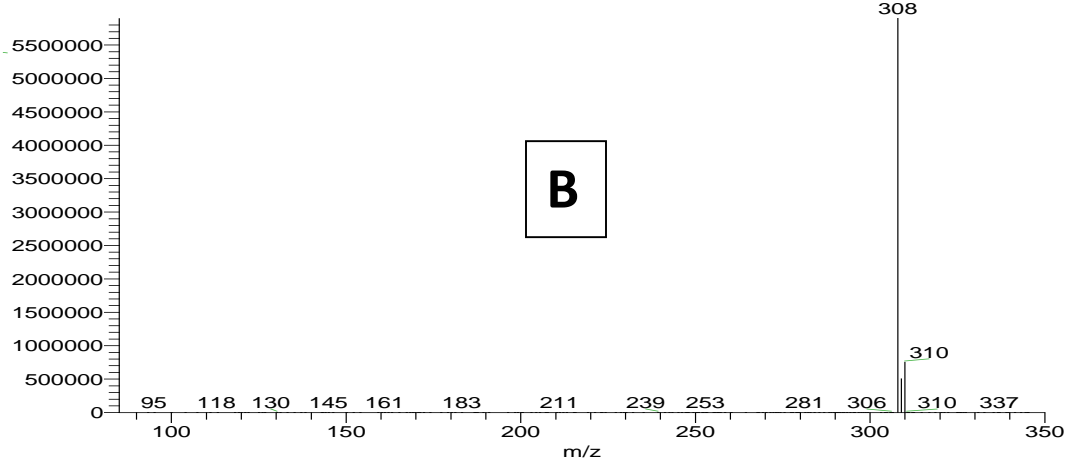
STD-101M_1 #9550 RT: 42.50 AV:
 F: ITMS + c ESI Full ms [80.00-400.00]

3-2.49 , 3.52-3.90 NL: 1.20E7



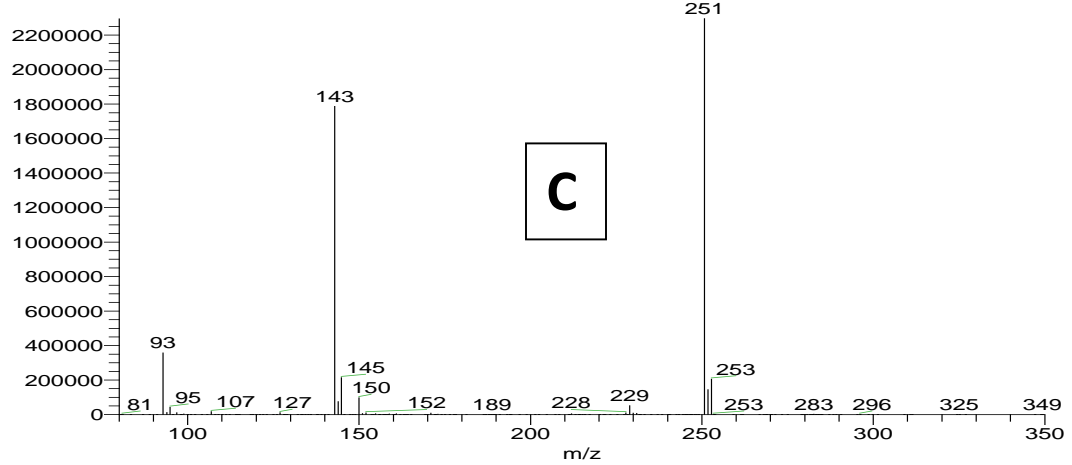
STD-101M_325 #4564-4723 RT: 40.1
 F: ITMS + c ESI Full ms2 325.00@cid

160 SB: 76 2.23-2.49 , 3.52-3.90 NL: 5.90E6
 0.00]



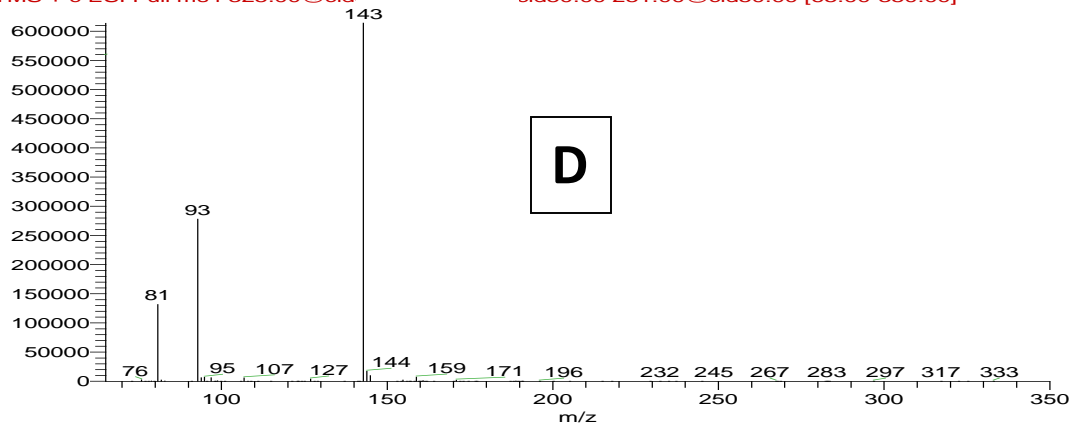
STD-101M_325-308 #3498-3554 RT:
 F: ITMS + c ESI Full ms3 325.00@cid

AV: 57 SB: 57 2.24-2.49 , 3.52-3.91 NL: 2.29E6
 cid50.00 [80.00-350.00]



STD-101M_325-308-251 #2701-2764
F: ITMS + c ESI Full ms4 325.00@cid

19 AV: 64 SB: 46 2.24-2.49 , 3.51-3.91 NL:
cid50.00 251.00@cid50.00 [65.00-350.00]



STD-101M_325-308-251-143 #2264-2
F: ITMS + c ESI Full ms5 325.00@cid

-41.61 AV: 46 SB: 38 2.24-2.49 , 3.51-3.91 NL:
cid50.00 251.00@cid50.00 143.00@cid50.00 [50.0 ...

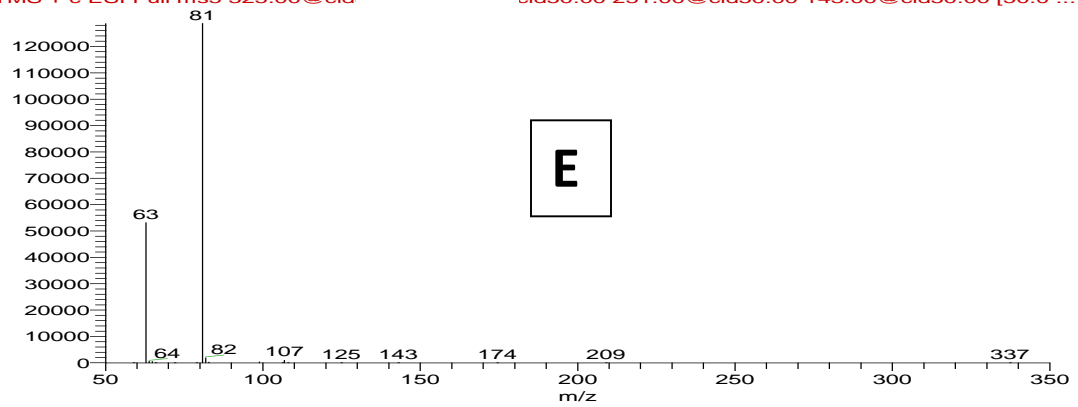
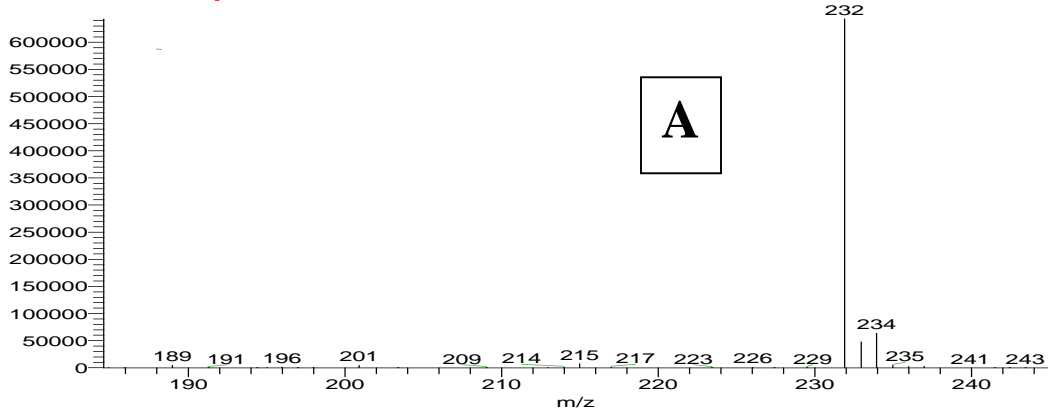


Figure 2s: Representative LC-MS spectra of $[M+NH_4]^+$, m/z 232, C-3 (A) Full Scan, (B) MS² and (C) MS³

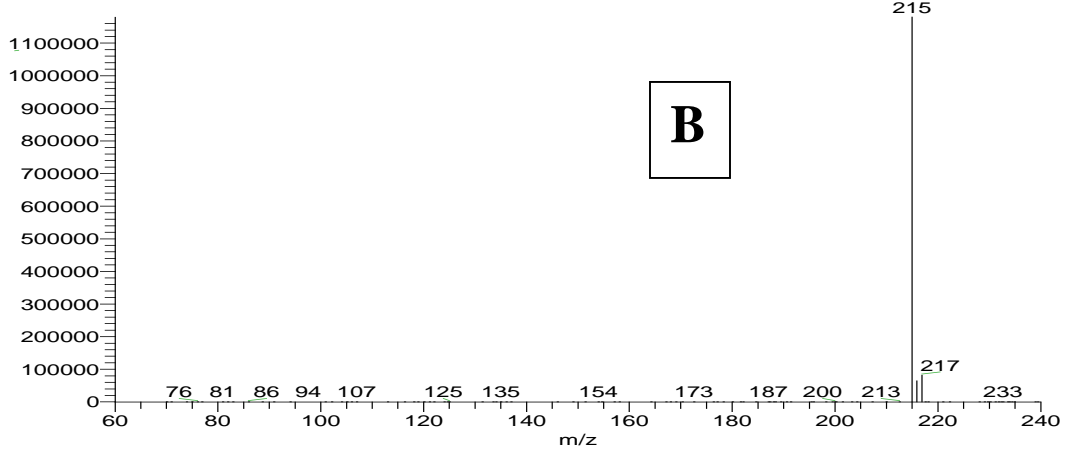
C14-101M-HLM-60min_1 #2277-2454
F: ITMS + c ESI Full ms [80.00-400.00]

07 AV: 178 SB: 152 2.23-2.49 , 3.52-3.90 NL:



C14-101M-HLM-120min_232 #825-88
F: ITMS + c ESI Full ms2 232.00@cid

0.63 AV: 59 SB: 52 2.23-2.49 , 3.52-3.91 NL:
0.00]



C14-101M-HLM-120min_232-215 #65
F: ITMS + c ESI Full ms3 232.00@cid

15-10.93 AV: 72 SB: 42 2.23-2.49 , 3.51-3.90 NL:
cid50.00 [55.00-240.00]

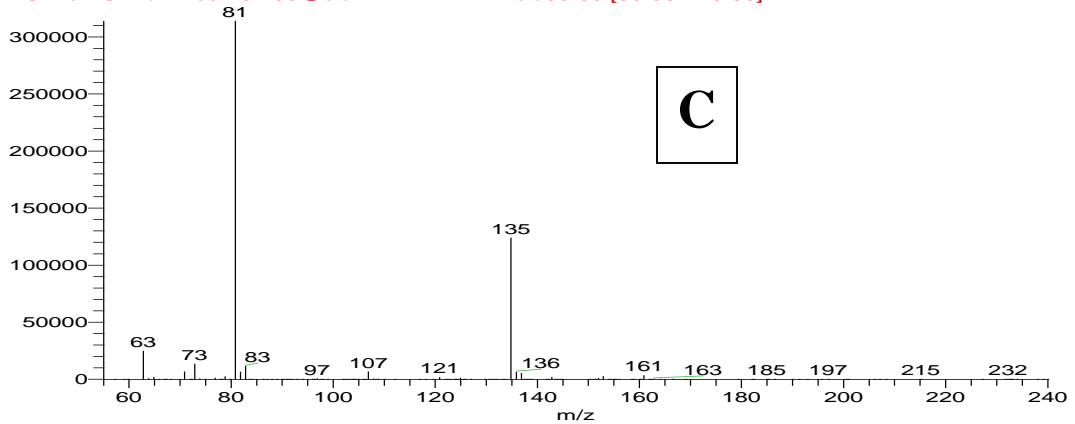
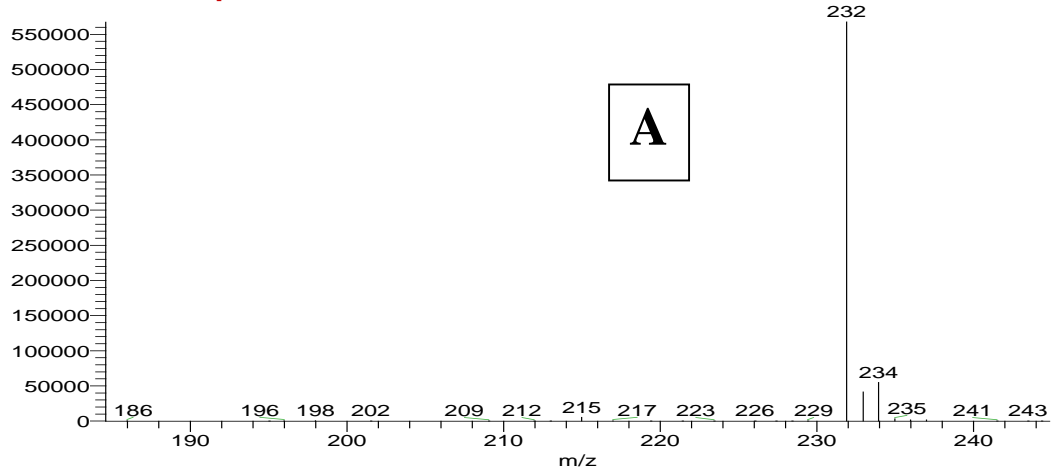


Figure 3s: Representative LC-MS spectra of $[M+NH_4]^+$, m/z 232, C-4 (A) Full Scan, (B) MS² and (C) MS³

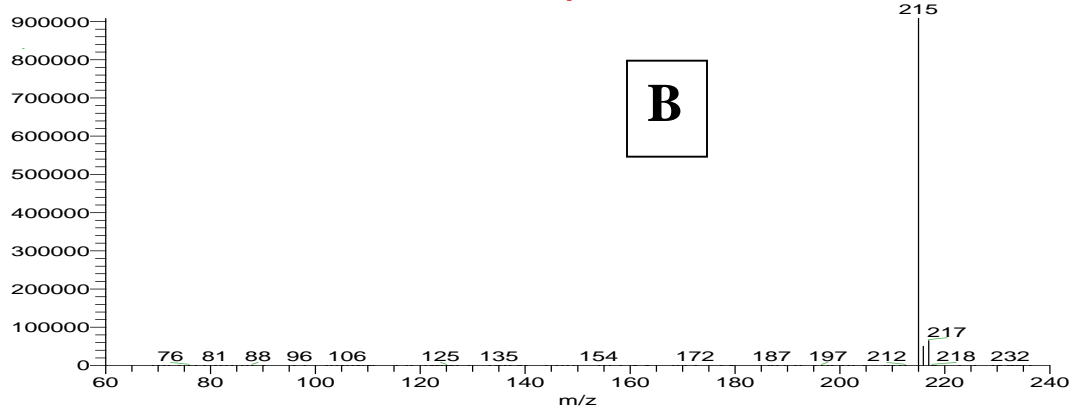
C14-101M-HLM-20min_1 #2755-2932
F: ITMS + c ESI Full ms [80.00-400.00]

14 AV: 178 SB: 152 2.23-2.49 , 3.52-3.90 NL:



C14-101M-HLM-120min_232 #1151-1:
F: ITMS + c ESI Full ms2 232.00@cid

-13.28 AV: 62 SB: 52 2.23-2.49 , 3.52-3.91 NL:
0.00]



C14-101M-HLM-120min_232-215 #85
F: ITMS + c ESI Full ms3 232.00@cid

29-13.02 AV: 67 SB: 42 2.23-2.49 , 3.51-3.90 NL:
cid50.00 [55.00-240.00]

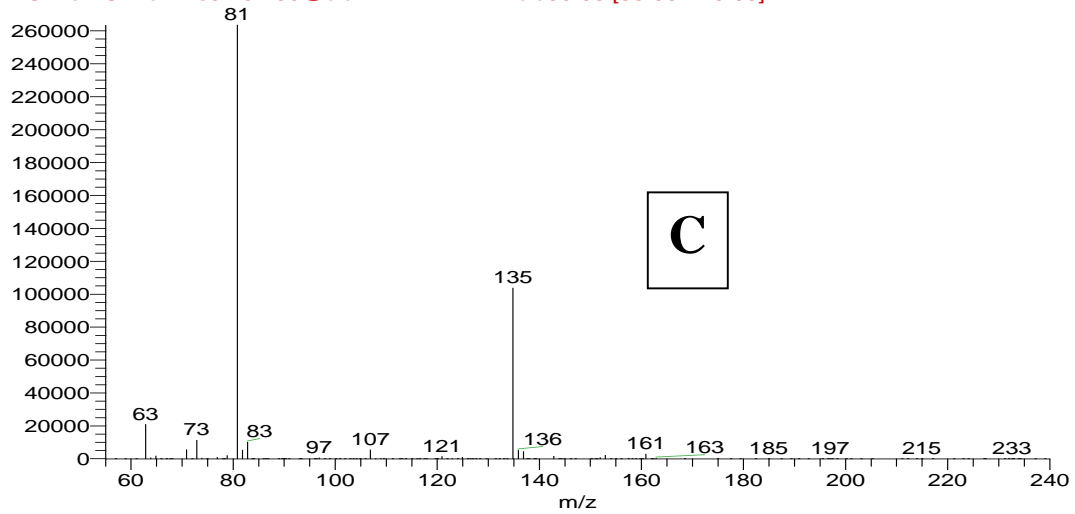


Figure 4s: Proposed structure and fragmentation ions for C-4

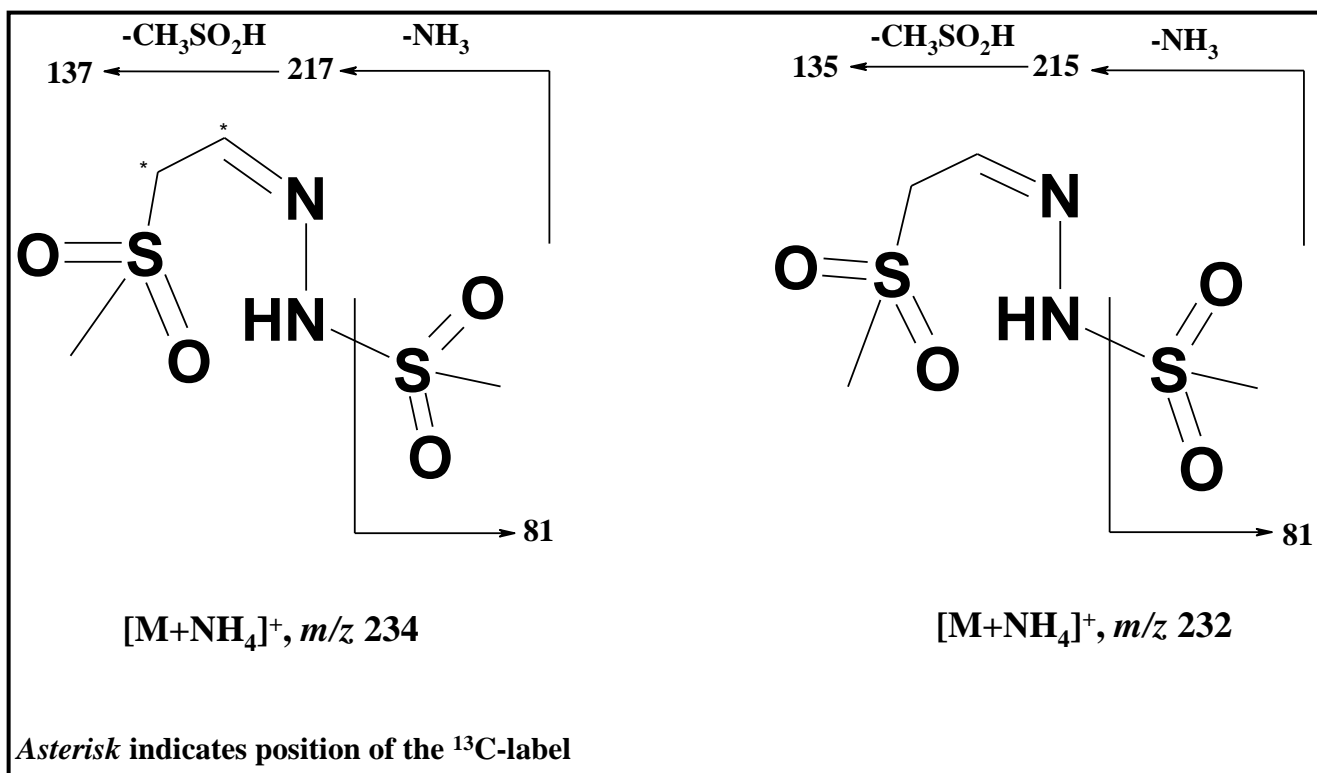


Figure 5s: Proposed structure and fragmentation ions for C-5

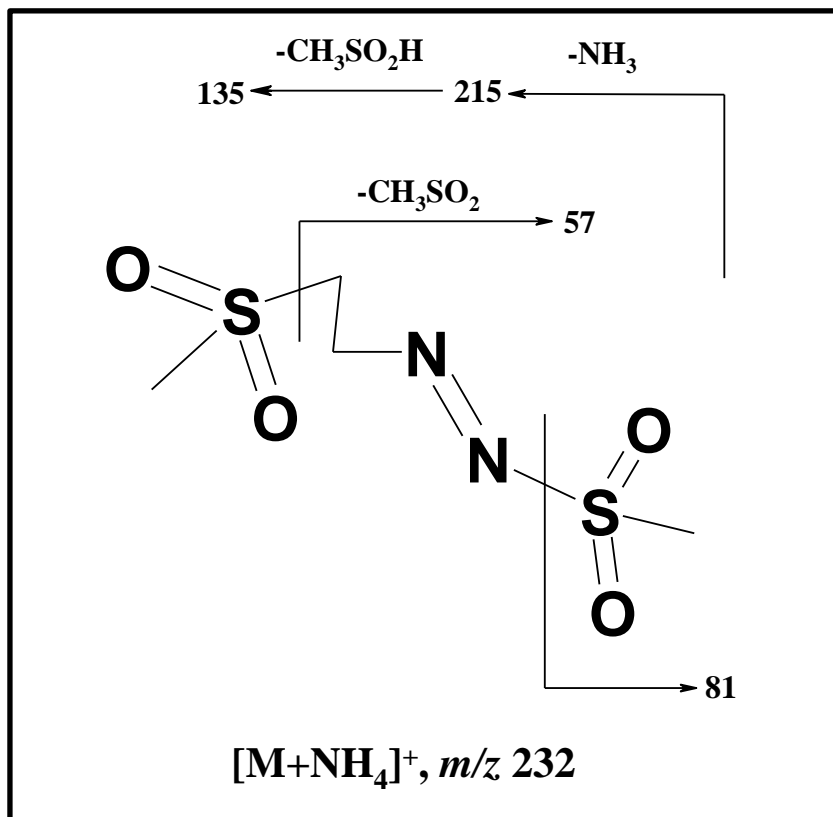
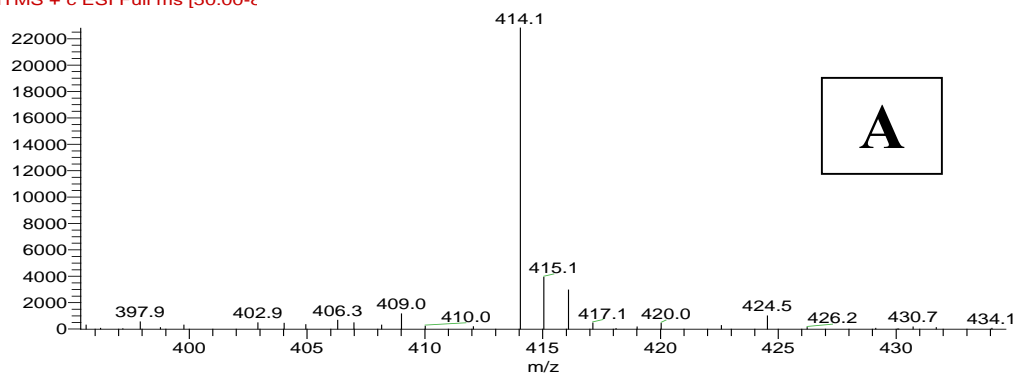
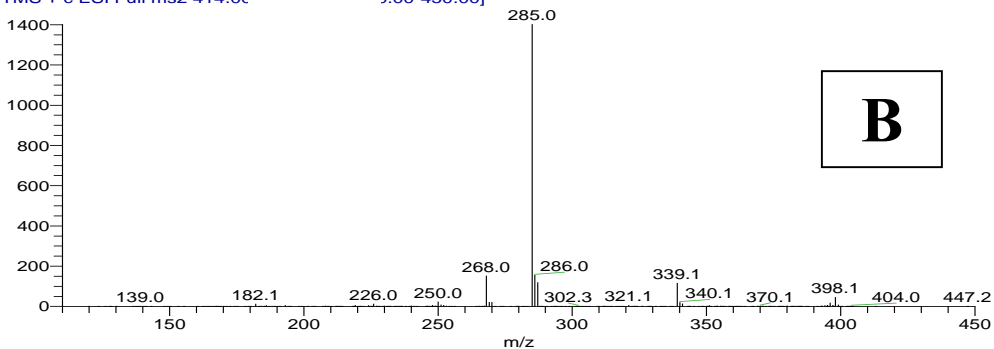


Figure 6s: LC-MS spectra of m/z 414, M-3 (A) full scan MS, (B) MS², (C) MS³, (D) MS⁴, and (E) MS⁵

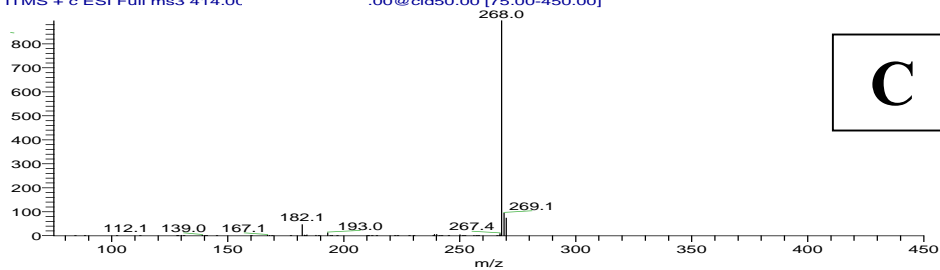
Jan7-90CE-C12-HLM-GSH-NAC-Cys-60min 414 #4254 RT: 27.88 AV: 1 SB: 2 16.66 , 17.49 NL: 2.28E4
 T: ITMS + c ESI Full ms [50.00-€



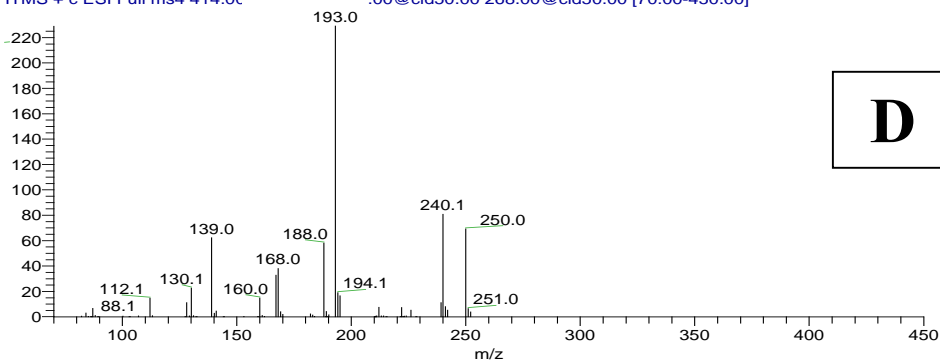
Jan7-90CE-C12-HLM-GSH-NAC-Cys-60min 414 #2083-2113 RT: 27.94-28.34 AV: 31 SB: 2 16.66 , 17.50 NL:
 T: ITMS + c ESI Full ms2 414.0€ (0.00-450.00]



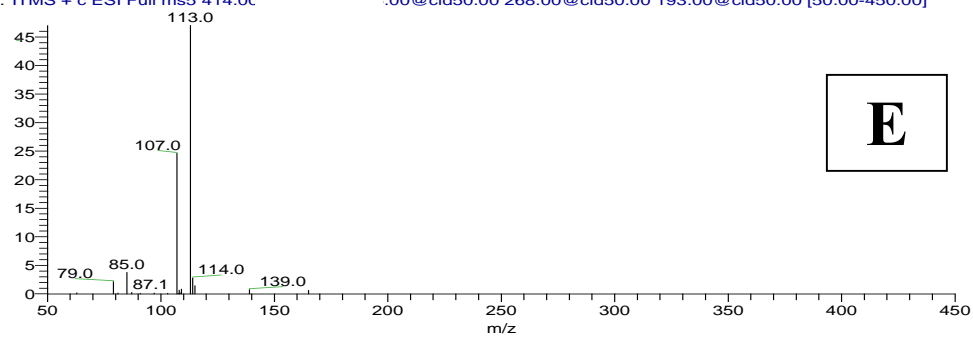
Jan7-90CE-C12-HLM-GSH-NAC-Cys-60min 414-285 #1690-1716 RT: 27.91-28.34 AV: 27 SB: 2 16.66 , 17.49 NL:
 T: ITMS + c ESI Full ms3 414.0€ (0.00@cid50.00 [75.00-450.00]



Jan7-90CE-C12-HLM-GSH-NAC-Cys-60min 414-285-268 #1428-1451 RT: 27.90-28.35 AV: 24 SB: 2 16.66 , 17.50
 T: ITMS + c ESI Full ms4 414.0€ (0.00@cid50.00 268.00@cid50.00 [70.00-450.00]



Jan7-90CE-C12-HLM-GSH-NAC-Cvs-60min 414-285-268-193 #1235-1254 RT: 27.91-28.34 AV: 20 SB: 2
T: ITMS + c ESI Full ms5 414.0c .00@cid50.00 268.00@cid50.00 193.00@cid50.00 [50.00-450.00]



E

Figure 7s: Proposed structure and fragmentation pattern for M-3

